

1 **Advancing Santorini's tephrostratigraphy: new glass geochemical data and**
2 **improved marine-terrestrial tephra correlations for the past ~360 kyrs**

3
4 Sabine Wulf^{a,b*}, Jörg Keller^c, Christopher Satow^d, Ralf Gertisser^e, Michael Kraml^{c,1},
5 Katharine M. Grant^f, Oona Appelt^g, Polina Vakhrameeva^b, Andreas Koutsodendris^b,
6 Mark Hardiman^a, Hartmut Schulz^h, Jörg Pross^b

7
8 ^a School of the Environment, Geography and Geosciences, University of Portsmouth, Portsmouth,
9 United Kingdom

10 ^b Paleoenvironmental Dynamics Group, Institute of Earth Sciences, Heidelberg University, Heidelberg,
11 Germany

12 ^c Department of Mineralogy-Geochemistry, Institute of Earth and Environmental Sciences, University
13 of Freiburg, Freiburg, Germany

14 ^d Department of Social Sciences, Oxford Brookes University, Oxford, United Kingdom

15 ^e School of Geography, Geology and the Environment, Keele University, Keele, United Kingdom

16 ^f Research School of Earth Sciences, The Australian National University, Canberra, Australia

17 ^g Helmholtz Centre Potsdam, GFZ German Research Centre for Geosciences, Section 3.6 Chemistry
18 and Physics of Earth Materials, Potsdam, Germany

19 ^h Department of Geosciences, University of Tübingen, Tübingen, Germany

20
21 *Corresponding author at: School of the Environment, Geography and Geosciences, University of
22 Portsmouth, Portsmouth, United Kingdom, *E-mail address*: sabine.wulf@port.ac.uk (S. Wulf)

23
24 ¹ Present address: Geothermal Engineering GmbH, Surface Exploration and Research, Karlsruhe,
25 Germany

26
27
28 **Keywords:** Santorini, EPMA glass chemistry, proximal tephra deposits, marine
29 tephrostratigraphy, land-sea correlations, Eastern Mediterranean region

30
31 **Abstract**

32 The island of Santorini in the Aegean Sea is one of the world's most violent active volcanoes.
33 Santorini has produced numerous highly explosive eruptions over at least the past ~360 kyrs
34 that are documented by the island's unique proximal tephra record. However, the lack of
35 precise eruption ages and comprehensive glass geochemical datasets for proximal tephras
36 has long hindered the development of a detailed distal tephrostratigraphy for Santorini
37 eruptions. In light of these requirements, this study develops a distal tephrostratigraphy for
38 Santorini covering the past ~360 kyrs, which represents a major step forward towards the
39 establishment of a tephrostratigraphic framework for the Eastern Mediterranean region. We
40 present new EPMA glass geochemical data of proximal tephra deposits from twelve Plinian
41 and numerous Inter-Plinian Santorini eruptions and use this dataset to establish assignments
42 of 28 distal marine tephras from three Aegean Sea cores (KL49, KL51 and LC21) to specific
43 volcanic events. Based on interpolation of sapropel core chronologies we provide new eruption
44 age estimates for correlated Santorini tephras, including dates for major Plinian eruptions,
45 Upper Scoriae 1 (80.8 ± 2.9 ka), Vourvoulos (126.5 ± 2.9 ka), Middle Pumice (141.0 ± 2.6 ka),
46 Cape Thera (156.9 ± 2.3 ka), Lower Pumice 2 (176.7 ± 0.6 ka), Lower Pumice 1 (185.7 ± 0.7 ka),
47 and Cape Therma 3 (200.2 ± 0.9 ka), but also for 17 Inter-Plinian events. Older Plinian and
48 Inter-Plinian activity between ~310 ka and 370 ka, documented in the distal terrestrial setting
49 of Tenaghi Philippon (NE Greece), is independently dated by palynostratigraphy and
50 complements the distal Santorini tephrostratigraphic record.

51

52 **1. Introduction**

53 Tephra (volcanic ash) layers in sedimentary records have long been used as dating tools in
54 Quaternary science (e.g., Thorarinsson, 1944; Lowe, 2011) and are today widely applied for
55 synchronising palaeoclimate proxy datasets on regional to supra-regional scales (e.g., Lane
56 et al., 2013; Wulf et al., 2013; Rach et al., 2014). However, an important prerequisite for
57 reliable dating and proxy-data linking via tephras is the availability of detailed
58 tephrostratigraphic frameworks for volcanic eruption centres. Ideally, these
59 tephrostratigraphies encompass complete sequences of past eruptive events in stratigraphic

60 order, high-precision dating, and comprehensive glass geochemical datasets of erupted
61 tephtras from proximal (i.e., near-vent) settings that enable detailed correlations with distal
62 deposits. In Europe, such tephrostratigraphies are well established for Holocene and Late
63 glacial Icelandic volcanoes (e.g., Larsen and Eiriksson, 2008; Lawson et al., 2012; Davies et
64 al., 2014; Gudmundsdóttir et al., 2016; Wastegard et al., 2018) and for the Italian volcanic
65 peninsula dating back to ~800 ka (e.g., Narcisi and Vezzoli, 1999; Wulf et al., 2004;
66 Santacroce et al., 2008; Zanchetta et al., 2011; Wulf et al., 2012; Insinga et al., 2014; Albert
67 et al., 2017; Giaccio et al., 2017a). In contrast, tephrostratigraphies are still fragmentary for
68 the Eastern Mediterranean region. This applies particularly to Aegean Arc volcanoes and
69 notably Santorini Island, which hosts one of the world's most explosive, still active volcanic
70 centres (e.g., Druitt et al., 1999). Santorini volcanism is particularly well known for its Late
71 Bronze Age or Minoan eruption at ~1600 BC, which represents one of the world's largest
72 volcanic eruptions in recorded history (e.g., Bond and Sparks, 1976; Sparks and Wilson, 1990;
73 Druitt et al., 1999; Friedrich et al., 2006). This eruption may have severely impacted the Late
74 Minoan civilisation in the Aegean region, with massive pumice fall and pyroclastic density
75 currents (PDCs) destroying the town of Akrotiri on Thera (Santorini) and a tsunami devastating
76 coastal towns on the nearby island of Crete (e.g., Marinatos, 1939; Antonopoulos, 1992;
77 Friedrich, 2000; Bruins et al., 2008).

78 The proximal tephra record on Santorini documents numerous Plinian and Inter-Plinian
79 eruptions during the past ~360 kyrs, but dating of the calc-alkaline products (tephtras) from
80 these eruptions has long been challenging, especially beyond the radiocarbon dating range.
81 This is because most radioisotopic dates derived from whole-rock K/Ar and multi-grain
82 $^{40}\text{Ar}/^{39}\text{Ar}$ methods produced large age uncertainties due to either inherited feldspar xenocrysts
83 and the generally low K-contents of Santorini eruption products (~0.1-3.8 wt% K_2O ; Druitt et
84 al., 1999), or high atmospheric contamination (on average >95%; Fabbro et al., 2013).
85 Furthermore, the low number of macroscopically visible Santorini tephtras in distal settings
86 such as in deep-sea cores from the Aegean and Levantine Seas (Keller et al., 1978; Federman
87 and Carey, 1980; Vinci, 1985) did not stimulate tephrostratigraphic studies in this region for a

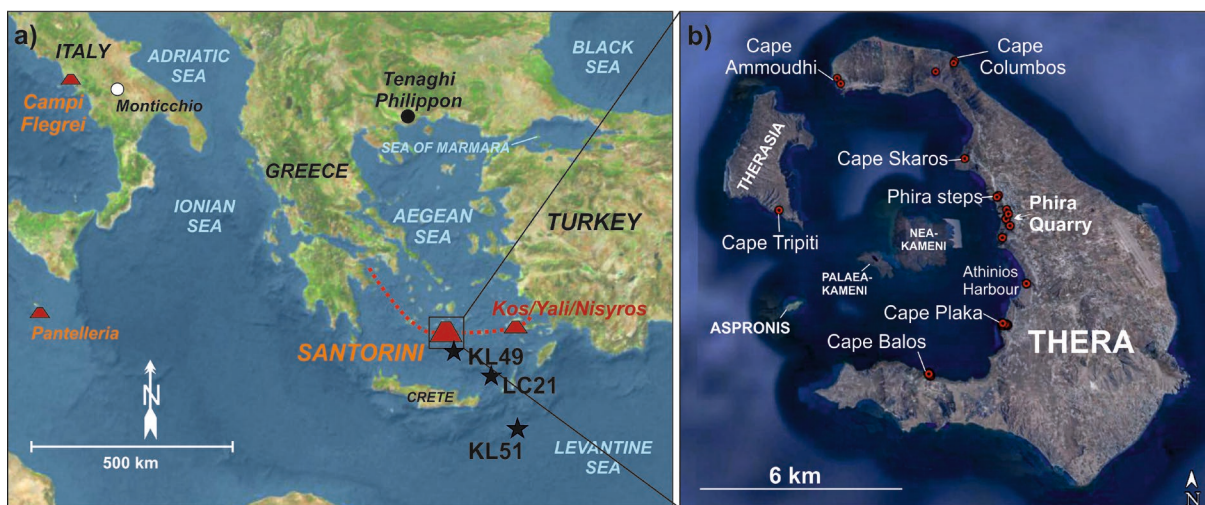
88 long time, leading to a focus of Santorini tephra on petrographical and bulk rock geochemical
89 characterisation rather than on glass compositions (e.g., Fouque, 1879; Reck, 1936; Druitt et
90 al., 1999; Vespa et al., 2006; Gertisser et al., 2009). Hence, EPMA glass geochemical data
91 available from the proximal record are either published as mean data (Federman and Carey,
92 1980; Keller, 1981; Vinci, 1985; Druitt et al., 1999; Gertisser et al., 2009) or comprise only
93 major eruptive units of the last ~100 kyrs (Tomlinson et al., 2015), highlighting a need for a
94 new comprehensive dataset.

95 Recent tephrostratigraphic studies of marine core LC21 from the SE Aegean Sea (Satow et
96 al., 2015) identified for the first time macroscopically non-visible (crypto)tephra layers of
97 Santorini provenance in the Eastern Mediterranean Sea. However, due to the lack of
98 comparative glass geochemical data, these cryptotephra have not yet been correlated to
99 specific volcanic events (Satow et al., 2015), which currently limits their use as isochronous
100 marker layers.

101 In recognition of the need of a comprehensive glass geochemical dataset, systematic
102 sampling and EPMA major-element analysis of all Plinian and a number of Inter-Plinian
103 deposits from the proximal tephra record on Santorini has been carried out for this study. The
104 new dataset has been employed to assign precise eruptions to the above-mentioned
105 (crypto)tephra dataset from core LC21 (Satow et al., 2015) and to the visible tephra records
106 of two other important Aegean Sea cores, namely cores M40/4-65 (GeoTÜ-KL49; hereafter:
107 KL49) and M40/4-67 (GeoTÜ-KL51; hereafter: KL51), to provide a complete marine-distal
108 Santorini tephrostratigraphic framework for the region southeast of Santorini for the last 200
109 kyrs (Schwarz et al., 1999; Keller et al., 2000; Schwarz, 2000). Furthermore, the original age
110 models of cores KL49 and KL51 as used by Schwarz (2000) and Keller et al. (2000) for
111 estimating ages for marine Santorini tephra have been revised using the latest chronological
112 information available for sapropel boundaries and other tephra markers. Independent dates
113 for older Santorini Plinian and Inter-Plinian activity between ~310 and 370 ka have been
114 derived through palynostratigraphic age constraints of several cryptotephra layers in the distal
115 terrestrial archive of Tenaghi Philippon, NE Greece (Vakhrameeva et al., 2018, 2019).

116 The new, ~360-kyr-long distal tephrostratigraphic record for Santorini facilitates reliable
 117 correlations of future Santorini-derived (crypto)tephra findings in marine and terrestrial
 118 palaeoenvironmental archives from the Eastern Mediterranean region. It furthermore helps to
 119 recognise Santorini events that are not preserved in the proximal record and provides new
 120 insights into Santorini's past eruptive behaviour, including the frequency and dynamics of large
 121 explosive events as well as tephra dispersal patterns, which are crucial for understanding and
 122 estimating the nature and frequency of future eruptive events.

123



124

125 **Figure 1: (a)** Topographic map of the Eastern Mediterranean region with locations of
 126 volcanoes and terrestrial sites of Lago Grande di Monticchio and Tenaghi Philippon (filled
 127 circles). Black stars indicate the positions of marine cores KL49, LC21 and KL51. Red dotted
 128 line shows the position of the southern Aegean volcanic arc. **(b)** Inlet satellite image of
 129 Santorini (Google Earth, 2018) with main proximal tephra sampling sites (see more details in
 130 Supplementary material S1). **(2-column fitting image)**

131

132 2. Santorini's eruptive history: the proximal record

133 Santorini is the largest and most active Quaternary volcanic centre within the southern Aegean
 134 volcanic arc (Fig. 1), which formed as a consequence of N-dipping subduction of the African
 135 plate underneath the European plate since the Miocene (e.g., Angelier et al., 1982; Mercier et
 136 al., 1989). Santorini consists of three major islands, Thera, Therasia and Aspronisi, which

137 encircle the central flooded caldera with the youngest twin islands of Palaea and Nea Kameni
138 (Fig.1). The Santorini volcanic complex, which formed over the last ≥ 650 kyrs (Druitt et al.,
139 1999), overlies a ca. 20-30 km thick continental crust of Mesozoic and Cenozoic metamorphic
140 rocks (e.g., Tartaris, 1964; Makris, 1978; Li et al., 2003; Druitt et al., 2015). Early shallow-
141 marine to subaerial volcanic activity produced dacitic to rhyodacitic lava flows from centres of
142 the Akrotiri Peninsula in the southwest of Thera Island (Druitt et al., 1999). These were
143 followed by effusive and minor explosive activity from the basaltic-andesitic Peristeria
144 composite volcano in northern Thera (530 – 430 ka; Druitt et al., 1999). Commencing around
145 the time of the last Peristeria activity, cinder and spatter cones were formed by Strombolian
146 eruptions on the Akrotiri Peninsula (450 – 340 ka; Druitt et al., 1999).

147 Major explosive volcanism started at ~ 360 ka; to date, this has resulted in twelve major
148 Plinian (Druitt et al., 1989; Druitt et al., 1999) and numerous Inter-Plinian explosive eruptions
149 (labelled M1 to M12) that have yet been rarely and only selectively studied (e.g., Edwards,
150 1994; Druitt et al., 1999; Vespa et al., 2006; Fabbro et al., 2013) (Fig. 2). Pumice and scoria
151 deposits from these events form the Thera Pyroclastic Formation (TPF) that is well exposed
152 in the caldera wall succession of the Santorini ring islands. The TPF has been subdivided into
153 two explosive cycles based on long-term trends in magma composition, with each cycle
154 starting with mafic to intermediate magmas and ending with a silicic, caldera-forming eruption
155 (Druitt et al., 1999). During the first explosive cycle between ~ 360 and 180 ka, five Plinian
156 eruptions took place, preceded and intercalated by minor explosive eruptions and lava-shield
157 formations at Cape Alai (364 ± 62 ka; Druitt et al., 1999) and Cape Alonaki (224 ± 5 ka; Druitt
158 et al., 1999) (Fig. 2). The oldest Plinian eruptions produced the andesitic and rhyodacitic
159 pyroclastic successions of Cape Therma 1 (CTM1), Cape Therma 2 (CTM2), and Cape
160 Therma 3 (CTM3). The eruption ages of CTM1 and CTM2 are roughly constrained to ≤ 360 ka
161 and ~ 225 ka based on $^{40}\text{Ar}/^{39}\text{Ar}$ dates of directly underlying Cape Alai (CTM1) and overlying
162 Cape Alonaki lavas (CTM2), respectively (Druitt et al., 1999) (Fig. 2). A first age estimate for
163 the CTM3 eruption of 196 ka was derived from interpolation of the proposed marine tephra
164 correlative “Intra-S7” by the original age model of Aegean Sea core KL51 (Keller et al., 2000;

165 Schwarz, 2000). The Cape Thera successions are overlain by the rhyodacitic Lower Pumice
166 1 (LP1) and Lower Pumice 2 (LP2) deposits (e.g., Druitt et al., 1989, 1999; Gertisser et al.,
167 2009; Simmons et al., 2016), both formerly assigned to the “Unterer Bimsstein” (Reck, 1936)
168 or “Lower Thera Pumice” (Keller, 1981). LP1 and LP2 were derived from relatively closely
169 spaced Plinian events that are separated by a thin palaeosol. LP1 and LP2 have been
170 proposed to be distally recorded in the KL51 marine record as V-3 and V-1 tephras, where
171 their ages were interpolated at 184 and 172 ka, respectively (Keller et al., 1978, 2000, 2014;
172 Schwarz, 2000). The LP2 eruption resulted in the collapse of Caldera 1 (Druitt et al., 1989,
173 1999; Gertisser et al., 2009), which was followed by the formation of the Simandiri lava-shield
174 (172 ± 4 ka; Druitt et al., 1999). Minor deposits of Inter-Plinian activity (M1 to M5) have been
175 noted for the first explosive cycle, but have yet remained scarcely investigated (Edwards,
176 1994; Druitt et al., 1999).

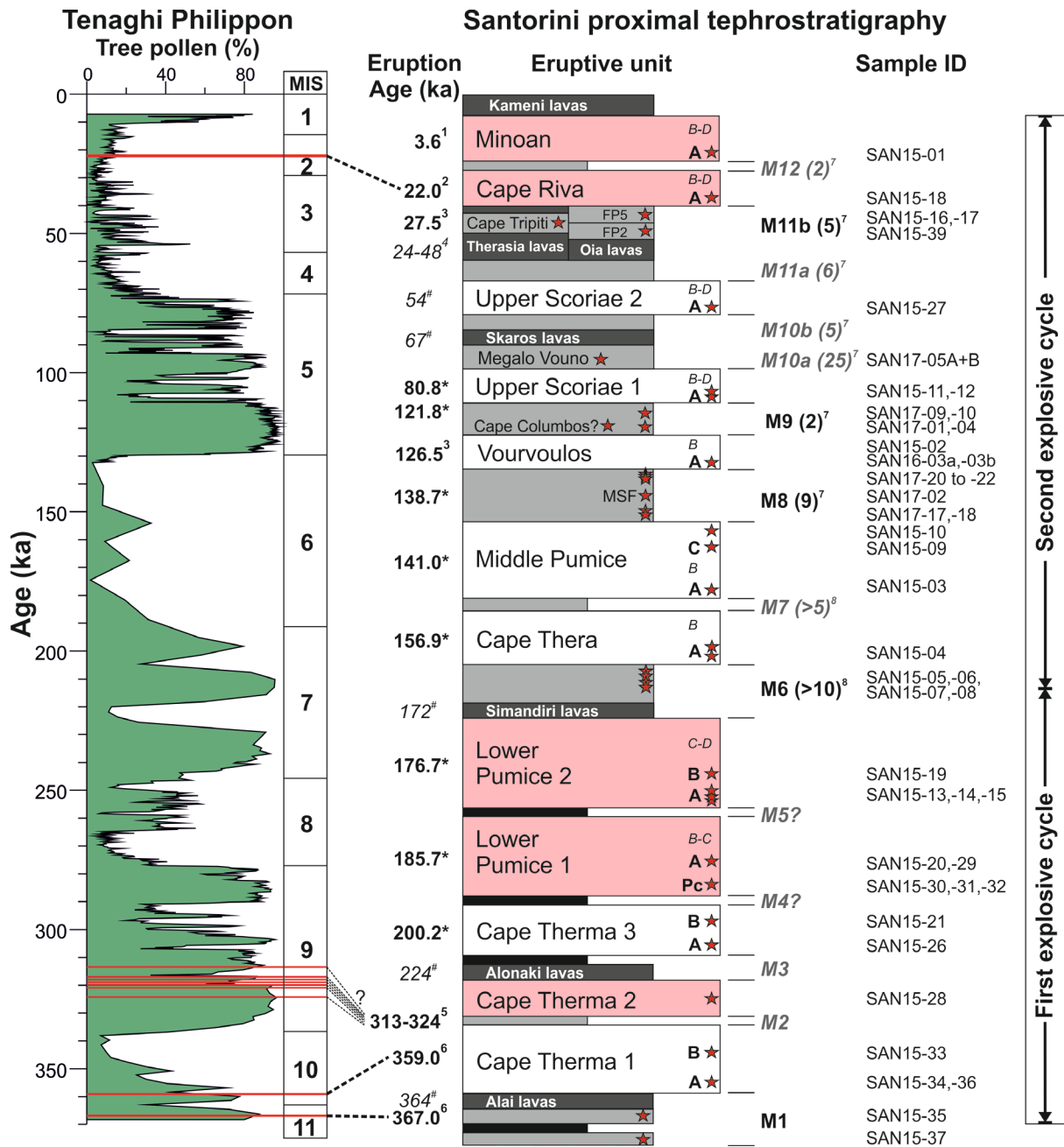
177 The second explosive cycle (~180 – 3.6 ka) started with the eruption of the Middle Tuff
178 Series, which encompasses andesitic to dacitic fall deposits and PDC deposits (ignimbrites)
179 from four major Plinian eruptions. These include the Cape Thera (CTA), Middle Pumice (MP),
180 Vourvoulos (V) and Upper Scoriae 1 (USC1) eruptions, all of which are intercalated by
181 relatively thick, mafic to intermediate ash and scoria beds from Inter-Plinian events (M6 to
182 M10; Druitt et al., 1999; Vespa et al., 2006). The Skaros caldera (Caldera 2) formed
183 incrementally during the Middle Tuff Series of eruptions and was established after the USC1
184 event. It was subsequently filled by the lava flows of the Skaros lava shield (67 ± 9 ka; Druitt
185 et al., 1999) in the northern part of Thera. Deposits of Plinian and Inter-Plinian eruptions of the
186 Middle Tuff Series all lack radioisotopic dating, but the first interpolated age estimates from
187 marine sapropels indicate eruption ages of 144.6 ± 2 ka for MP (marine W-2 tephra) and $80 \pm$
188 2 ka for USC1 (marine X-1 tephra; Keller et al., 2000; Schwarz, 2000).

189 This time interval of the eruption of the Middle Tuff Series has also been considered for the
190 formation of the Megalo Vouno cinder cone and Cape Columbus tuff ring that occurred along
191 the NE-SW striking Columbus tectonic line in NE Thera (Druitt et al., 1999). Reliable
192 radioisotopic ages for these eruptions are not yet available; however, the stratigraphic position

193 of the Megalo Vouno scoria deposits relative to Plinian deposits of the Middle Tuff Series
194 suggests a timing of this event between the Vourvoulos eruption and the Skaros lava-shield
195 formation (Druitt et al., 1999; Vespa et al., 2006). Furthermore, petrological similarities suggest
196 an even more specific allocation within the early M10a Inter-Plinian interval, i.e., after the
197 eruption of USC1 and prior to the Skaros lavas (Vespa et al., 2006). The phreatomagmatic
198 nature of the Cape Columbos tuff ring, on the other hand, implies that this likely formed at a
199 time when sea level was comparable to today's, i.e. during the last interglacial period (MIS 5e;
200 Druitt et al., 1999).

201 The Middle Tuff Series and the Skaros lava shield are succeeded by the andesitic deposits of
202 the major Upper Scoriae 2 eruption (USC2) that is dated by several means, i.e. by K/Ar whole
203 rock at 79 ± 8 ka, by $^{40}\text{Ar}/^{39}\text{Ar}$ whole rock at 54 ± 3 ka (Druitt et al., 1999), and by radiocarbon
204 determinations on organic material underlying the USC2 deposit at 37.9 ± 0.2 ^{14}C ka BP
205 (Mellors and Sparks, 1991). The USC2 event is followed by the extrusion of rhyodacitic lavas
206 forming the Therasia dome complex exposed on Therasia and Thera (48 – 24 ka; Fabbro et
207 al., 2013), and the thin andesitic lava flows at Oia in northern Thera that occur in the same
208 stratigraphic level as the Therasia lavas. On Therasia, the upper part of the lava succession
209 is intercalated by the silicic Cape Tripiti pumice deposit (26 ka; Fabbro et al., 2013). At Cape
210 Ammoudhi in northern Thera, five discrete, thin pumice fall deposits (FP1 to FP5) overly the
211 Oia lavas (Vespa et al., 2006); their chronostratigraphic relationship to the Cape Tripiti Pumice
212 is yet unclear.

213 The second explosive cycle terminated with the two rhyodacitic, caldera-forming Cape Riva
214 (CR, Caldera 3; Druitt and Sparks, 1982; Druitt, 1985) and the Late Bronze Age or Minoan
215 eruptions (MIN, Caldera 4; e.g., Bond and Sparks, 1976; Sparks and Wilson, 1990; Druitt et
216 al., 1999) (Fig. 2). Both eruptions formed prominent pyroclastic fall and PDC deposits, and are
217 radiocarbon-dated at 22.0 ± 0.6 cal ka BP (2σ uncertainty; Pichler and Friedrich, 1976; Bronk
218 Ramsey et al., 2015) and 1613 ± 13 cal a BC (3563 ± 13 cal a BP; Friedrich et al., 2006),
219 respectively. Historic effusive activity has built the present-day islands of Palaea Kameni and
220 Nea Kameni, with the last eruption taking place in AD 1950 (Fytikas et al., 1990).



221

222

223

224

225

226

227

228

229

Figure 2: Left: Tree-pollen curve of the Tenaghi Philippon peat record (NE Greece) for the past ca. 370 kyrs with positions of Marine Isotope Stages (MIS) and (crypto)tephra layers of Santorini provenance (red lines). Data from Pross et al. (2009, 2015), Müller et al. (2011), Fletcher et al. (2013), Milner et al. (2016), Wulf et al. (2018), and Vakhrameeva et al. (2018, 2019). Right: Revised Santorini proximal eruptive history showing Plinian events (white fields = intermediate composition, red field = silicic composition), Inter-Plinian activity (light grey fields), lava-shield (dark grey fields) and soil formation (black fields); modified after Druiitt et al. (1999). Ages of eruptions are obtained from: ¹ Friedrich et al. (2006), ² Bronk Ramsey et al. (1999).

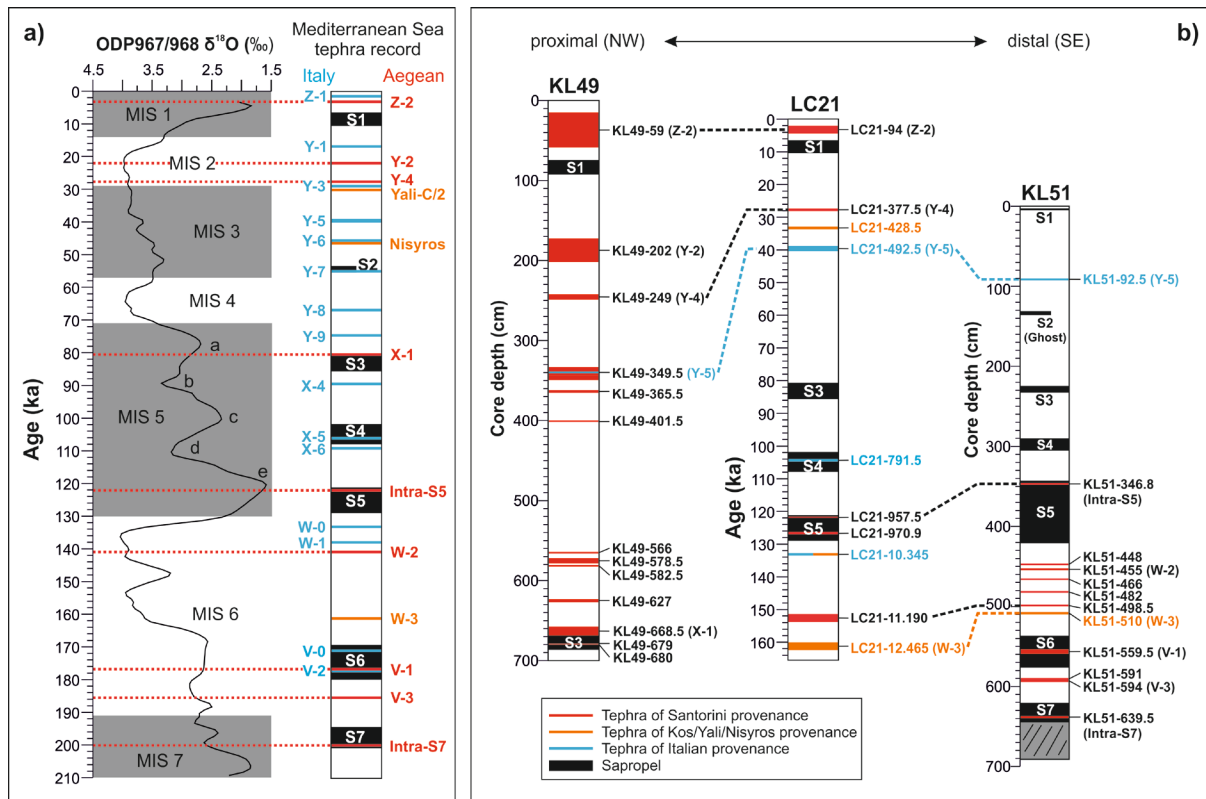
230 al. (2015), ³ Satow et al. (2015), ⁴ Fabbro et al. (2013), ⁵ Vakhrameeva et al. (2019), ⁶
231 Vakhrameeva et al. (2018), [#] Druitt et al. (1999) and ^{*} this study. Red stars show the
232 stratigraphic position of proximal tephra samples taken for this study, and respective tephra
233 sample IDs are listed on the right. Inter-Plinian (M) deposits in bold indicate intervals that have
234 been analysed in this study. Numbers in brackets behind M deposits indicate the number of
235 recognised Inter-Plinian units as estimated by ⁷ Vespa et al. (2006) and ⁸ Edwards (1994).
236 Note that this number is not representative for the number of distinct eruptions. **(2-column**
237 **fitting image)**

238

239 **3. Santorini's distal tephrostratigraphic record: state of the art**

240 Explosive activity on Santorini during at least the last ~360 kyrs has produced large volumes
241 of fallout tephra in the proximal record, and hence has the potential for distal dispersal.
242 Research on Santorini's distal tephrostratigraphy was initiated in the 1960s by the first
243 detection of the Minoan (Z-2) tephra in Eastern Mediterranean deep-sea sediments (e.g.,
244 Ninkovich and Heezen, 1965, 1967; Keller and Ninkovich, 1972; Keller et al., 1978; Watkins
245 et al., 1978; Vinci, 1985), on the islands of Crete, Milos and Rhodes (e.g., Vitaliano and
246 Vitaliano, 1974; Doumas and Papazoglou, 1980; Bruins et al., 2019), and in Asia Minor (e.g.,
247 Sullivan, 1988). Subsequent studies of marine sediment cores from the southern Aegean and
248 Levantine Seas identified six further visible tephra layers of Santorini provenance in deeper
249 stratigraphic positions that, according to their occurrence in different foraminiferal stratigraphic
250 zones, are labelled as Y-2 (CR), Y-4 (Cape Tripiti), X-1 (USC1), W-2 (MP), V-1 (LP2) and V-
251 3 (LP1) tephras (e.g., Keller et al., 1978; Federman and Carey, 1980; Vinci, 1985; Fabbro et
252 al., 2013) (Fig. 3).

253



254

255 **Figure 3:** (a) Benthic oxygen-isotope splice from ODP Sites 967/968 in the Eastern
 256 Mediterranean Sea (Konijnendijk et al., 2015) with positions of marine isotope stages (left)
 257 and revised Eastern Mediterranean marine tephrostratigraphic record for the last ~210 kyrs
 258 (right). Time constraints for sapropels S1 to S7 are from Grant et al. (2016, 2017). (b)
 259 Sediment logs of marine cores KL49, LC21 and KL51 with positions of tephra layers analysed
 260 and discussed in this study adapted from Hieke et al. (1999), Schwarz (2000), and Satow et
 261 al. (2015). (2-column fitting image)

262

263 During the past two decades, new findings at distal marine, but also at terrestrial sites from
 264 the northern Aegean Sea region (e.g., St. Seymour et al., 2004; Margari et al., 2007; Aksu et
 265 al., 2008; Wulf et al., 2018), the Sea of Marmara (e.g., Wulf et al., 2002; Çagatay et al., 2015),
 266 the Black Sea (Guichard et al., 1993; Kwiecien et al., 2008; Cullen et al., 2014), and Turkey
 267 (e.g., Eastwood et al., 1999; Roeser et al., 2012; Sulpizio et al., 2013) have extended the
 268 known dispersal fan of the younger Z-2 and Y-2 tephras. However, this does not hold true for
 269 older distal marker tephras (i.e., X-1, W-2, V-1, V-3). Notably, all distal findings have so far

270 been restricted to macroscopically visible layers of the above-mentioned eruptions, hence
271 providing no new insights into the eruption dynamics and tephra dispersal patterns of other,
272 likely less energetic Santorini eruptive events.

273 Satow et al. (2015) demonstrated for the first time the potential of detailing the distal Santorini
274 tephrostratigraphic record through the systematic cryptotephra analysis of core LC21 from the
275 SE Aegean Sea spanning the past ~160 kyrs (Fig. 3). Furthermore, ongoing studies of the
276 long Tenaghi Philippon (TP) peat sequence in NE Greece have highlighted the presence of
277 older Santorini cryptotephtras, some of which have been correlated with the Cape Therma 1
278 eruption, and M1 and M2 Inter-Plinian activity based on the proximal Santorini glass dataset
279 presented here (Vakhrameeva et al., 2018; 2019) (Fig. 2).

280 The first Santorini cryptotephra findings in palaeoclimate archives of the Aegean region mark
281 a turning point in the development of a more detailed Santorini tephrostratigraphy, but also
282 highlight the need for a comprehensive proximal Santorini glass geochemical dataset for
283 reliable tephra correlations.

284

285 **4. Material and Methodologies**

286 **4.1 Sampling and analysis of proximal tephtras from Santorini**

287 For this study, the sampling of proximal Santorini tephra deposits concentrated on pyroclastic
288 fall units in order to facilitate correlations with air-borne distal tephra layers.

289 In total, 49 tephra samples were taken during three field campaigns on Santorini in September
290 2015, November 2016 and April 2017 (samples “SAN15”, “SAN16” and “SAN17”,
291 respectively). Sampling encompassed mainly the basal fall units of all twelve major Plinian
292 and 25 of the most prominent fall units of the M11b, M9, M8, M6 and M1 Inter-Plinian intervals,
293 including deposits from the Megalo Vouno cinder cone and the Cape Columbus tuff ring. In
294 addition to basal fall units, samples from PDC (ignimbritic) sub-units of three of the older
295 Plinian eruptions (CTM1, CTM3, and LP2) have been taken since those could have potentially
296 produced distal co-ignimbritic ash fall with different glass chemical compositions. This may
297 also hold true for PDC units of other Plinian eruptions, i.e., LP1, CTA, MP, V, USC1, and

298 USC2, which have not been sampled for this study. However, in order to guarantee reliable
299 marine tephra correlations with their proximal counterpart, unpublished USC2-B glass data of
300 Schwarz (2000) and mean EDS analyses of other relevant missing PDC units from Druitt et
301 al. (1999) have been taken into account for comparison (Figs. 7-9).

302 For this study, most of the sampled proximal tephra fall deposits were accessible at the caldera
303 cliffs of Thera (e.g., Cape Ammoudhi, Cape Plaka, Cape Balos, Phira Steps) and Therasia
304 (Cape Tripiti), or at road cuts and quarries (e.g., Phira Quarry). Details of all sampling sites
305 are provided in Supplementary material S1.

306 Representative juvenile clasts (pumice and scoria fragments) were sampled vertically across
307 the individual deposits, then rinsed in the laboratory with deionized water, dried, crushed and
308 sieved. Glassy material from the 20 – 100 μm (SAN15 samples) and 25 – 125 μm (SAN16
309 and SAN17 samples) fractions was embedded in resin (Epofix), sectioned and polished for
310 geochemical analysis.

311 The major element composition of individual glass shards from samples SAN15 ($n>20$) was
312 obtained by electron probe microanalyses (EPMA) at the GFZ German Research Centre for
313 Geosciences in Potsdam using a JEOL-JXA 8320 (WDS) probe with five spectrometers.
314 Analytical setups during these measurements were 15 kV accelerating voltage and a 10 nA
315 beam current, and a 5 – 10 μm beam was used (Supplementary material S2). Count times per
316 element were 20 seconds for Fe, Mn, Ti, Mg, P, and Cl, and 10 seconds for Si, Al, K, Ca, F,
317 and Na (measured first). Instrumental calibration and data quality verification prior to sample
318 analyses used common mineral standards, Max Planck Institute (MPI) glass standards
319 (ATHO-G, StHs6/80 and GOR-132; Jochum et al., 2006) and the natural Lipari obsidian (Hunt
320 and Hill, 1996; Kuehn et al., 2011).

321 Major element glass concentrations of SAN16 and SAN17 samples were measured at the
322 Natural History Museum, London. Analytical conditions used a 5-spectrometer CAMECA
323 SX100 microprobe with an accelerating voltage of 20 kV, a beam current of 20 nA and a
324 defocused beam of 10 μm diameter in order to minimise volatile loss. Count times per element

325 were 30 seconds except for Na (12 s, and measured first), P and Mn (60 s), and Cl (50 s).
326 MPI glass standards StHs6/80 and ATHO-G (Jochum et al., 2006) were analysed at the start,
327 during and at the end of the run to monitor analysis accuracy and precision. Analytical data of
328 SAN15, SAN16 and SAN17 samples were filtered to remove analyses of non-vitreous material
329 (i.e., microlites) and those that yielded analytical totals lower than 95 wt% (mafic-intermediate
330 compositions) and 90 wt% (rhyolitic glass compositions), respectively. For data comparison in
331 bivariate elemental plots (Figs. 5, S1-3, S1-8, S1-11, S1-14, S1-19 and S1-22 in Supplement
332 material S1) analytical data were normalised to 100 wt%. All raw and normalised geochemical
333 data including glass standard data are provided in Supplementary material S2.

334

335 **4.2 Sampling and analysis of distal marine tephras**

336 **4.2.1 Deep-sea cores KL49 and KL51 (SE Aegean Sea)**

337 During R/V METEOR cruise M40/4 in January 1998, several deep-sea cores were collected
338 from the Aegean Sea for palaeoceanographic investigation (Hieke et al., 1999). Two of these
339 cores, KL49 and KL51 (M40/4-65 and M40/4-67 in Hieke et al., 1999), from medial-distal to
340 distal locations southeast of Santorini (Fig. 1) were tephrochronologically analysed by
341 Schwarz (2000), and respective data are presented here. Cores KL49 and KL51 have been
342 chosen for this study because they contain (1) numerous macroscopically visible tephra
343 layers, (2) well-preserved sapropels, and (3) undisturbed sediments with very limited
344 indications of reworking (e.g., turbidites) and bioturbation. All these criteria are important for
345 constructing reliable age models and eventually developing precise tephrostratigraphies.

346 Piston core KL49 was retrieved from a morphological high at 827 m water depth, ca. 30 km
347 south-southeast of Santorini (N36°08'46.2", E25°33'51.6"). Core KL51 was recovered from a
348 trough in 2158 m water depth, ca. 250 km southeast of Santorini (N34°48'49.8", E27°17'46.2").
349 The cores comprise 7 m and 6.91 m of marine sediments and extend back to sapropels S3
350 (KL49; ~87 ka) and S7 (KL51; ~200 ka), respectively (see Hieke et al., 1999, for detailed core
351 descriptions).

352 Glass geochemical data of 13 (KL49) and ten (KL51) Santorini tephras, in addition to two
353 other-sourced tephras from Schwarz (2000), have been used for this study and labelled
354 according to their core name and basal depth in cm, for example KL49-59 (Fig. 3;
355 Supplementary material S3). Marine tephra samples were sieved into 36-150 µm grain size
356 fractions, and liquid density and magnetic separation were applied to remove magnetic
357 minerals and organic material. Geochemical compositions of tephra glass shards were
358 determined using a CAMECA SX100 electron microprobe (WDS) at Institute of Earth and
359 Environmental Sciences, Freiburg (Germany), using a 15 kV accelerating voltage, 10 nA beam
360 current, and a defocused beam of 10 µm diameter (Supplementary material S3). Peak
361 counting times for each element were 20 s except for Na, which was analysed first at 10 s.
362 Instrumental calibration used International mineral and obsidian standards such as USNM
363 7285, KN18, and KE12 (Nielsen and Sigurdsson, 1981; Devine et al., 1995). Comparable
364 methods as for the proximal glass dataset were applied for filtering and normalising major
365 element data of marine tephras (Figs. 7-9, Supplementary material S3).

366

367 **4.2.2 Deep-sea core LC21 (SE Aegean Sea)**

368 Core LC21 was collected in 1995 during Marion Dufresne cruise 81 from 1522 m water depth,
369 ca. 130 km southeast of Santorini (N35°40', E26°35') (e.g., De Rijk et al., 1999; Hayes et al.,
370 1999). Sedimentological and geochemical studies of this ~14 m long core have shown that it
371 is excellently suited for high-resolution palaeoceanographic reconstructions for the past ~160
372 kyrs (e.g., Rohling et al., 2002, 2004; Casford et al., 2003; Marino et al., 2007, 2009; Abu-Zied
373 et al., 2008; Grant et al., 2012, 2016). Furthermore, LC21 documents several visible tephra
374 layers from Italian and Aegean Arc eruptions, and it is the first marine record in the Eastern
375 Mediterranean Sea that has been studied for its cryptotephra content (Satow et al., 2015). A
376 total of three visible and two cryptotephra layers has been geochemically assigned to Santorini
377 eruptions (Fig. 3), three of which still lack detailed correlations (Satow et al., 2015). Labelling
378 used the same approach as for tephras in the KL49 and KL51 cores (Figs. 7-9, Supplementary
379 material S3).

380

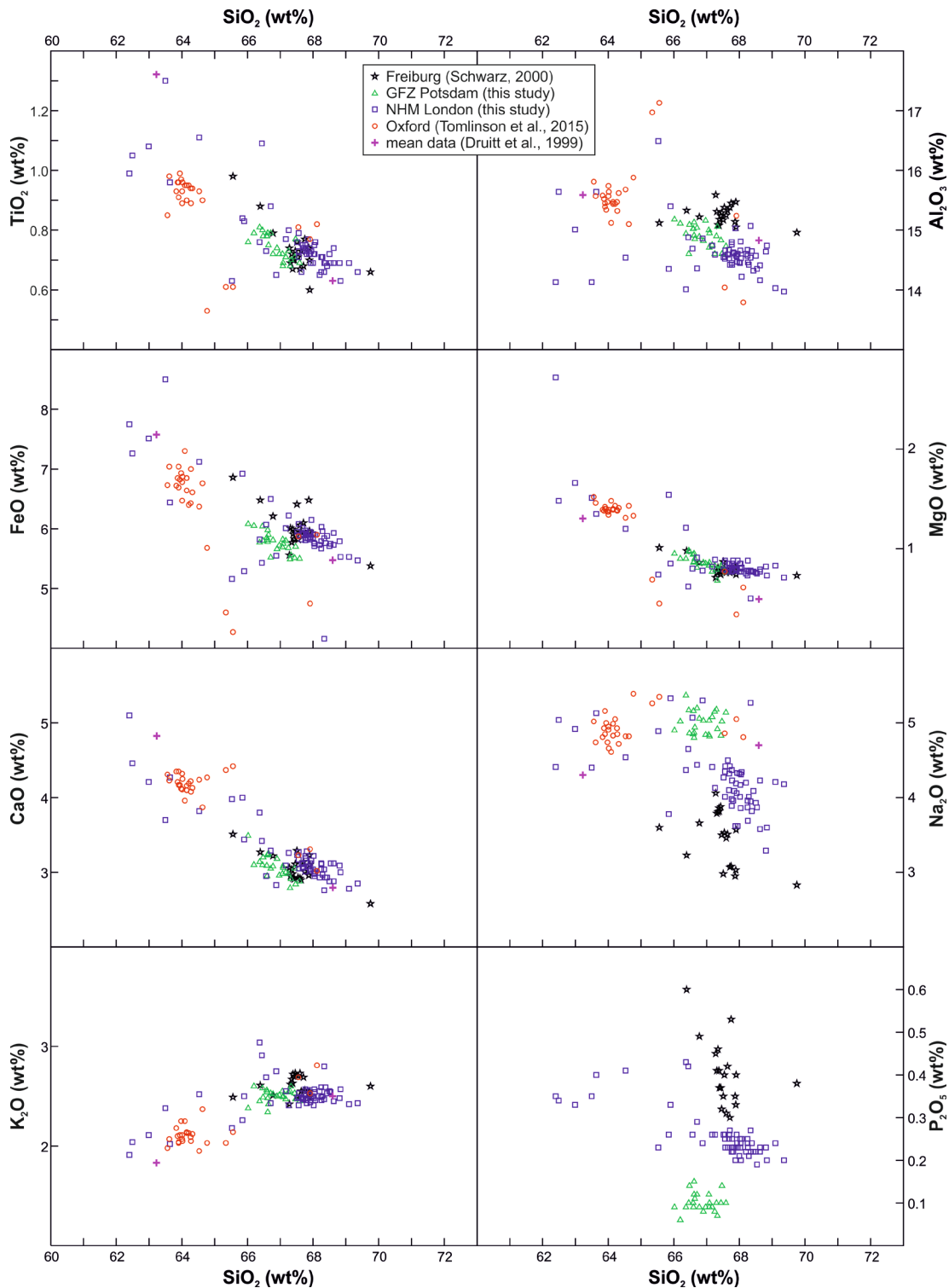
381 ***Please place Table 1 here (whole page width, portrait)***

382

383 **4.3 Comparability of proximal and marine distal EPMA glass data**

384 The new Santorini proximal tephra glass dataset was used for detailed correlations with the
385 glass chemical data of marine tephtras from cores KL49, KL51 (Schwarz, 2000; this study) and
386 LC21 (Satow et al., 2015). However, proximal and marine tephtras have been analysed by
387 using four different instruments with different analytical setups (Table 1), and hence the level
388 of comparability of data needs to be tested. The common use of glass standards for ensuring
389 EPMA data quality and comparability (e.g., Kuehn et al., 2011; Lowe et al., 2017), is in this
390 study, however, complicated by the fact that different glass standards were used during older
391 (Freiburg) and recent measurements (GFZ Potsdam, NHM London, Oxford) (Table 1).
392 Therefore, EPMA data of the proximal Vourvoulos fall (V-A) tephra have been used to evaluate
393 elemental difference within a mutual sample measured by all four laboratories (Fig. 4). The
394 comparison shows, on the one hand, that the new proximal glass datasets from the GFZ
395 Potsdam and NHM London laboratories agree well with each other except for slight deviation
396 in SiO₂, Na₂O and P₂O₅ values (Fig. 4). The Oxford data by Tomlinson et al. (2015) that used
397 the same analytical setup as for the marine LC21 tephtras (Satow et al., 2015) deviate from
398 the more homogeneous GFZ Potsdam data but overlap with the more scattered data of NHM
399 London data (Fig. 4). On the other hand, an unpublished glass dataset of the Vourvoulos
400 proximal tephra from Schwarz (2000) that used the same EPMA instrumental setups as for
401 marine KL49 and KL51 tephtras (Freiburg) shows significant deviations in Na₂O and P₂O₅
402 values and slightly higher SiO₂ concentrations compared to the new EPMA datasets (GFZ
403 Potsdam, NHM London) but agrees well for other elements, including TiO₂, FeO, MgO, CaO
404 and K₂O (Fig. 4). The deviations in SiO₂ and Na₂O are interpreted as a result from Na-loss
405 during EPMA measurements at the Freiburg instrument, and hence these elements have been
406 either excluded (Na₂O) or handled with caution (SiO₂) for proximal-distal tephra correlations.
407 In order to accommodate the comparability of SiO₂ data (one of the most important element

408 for tephra identification), we have included the unpublished proximal dataset of (Schwarz,
 409 2000) in all bivariate elemental plots next to the GFZ Potsdam and/or NHM London proximal
 410 data. This allowed for the more precise assignment of KL49 and KL51 marine tephras to their
 411 proximal counterparts (Figs. 7-9).
 412



413

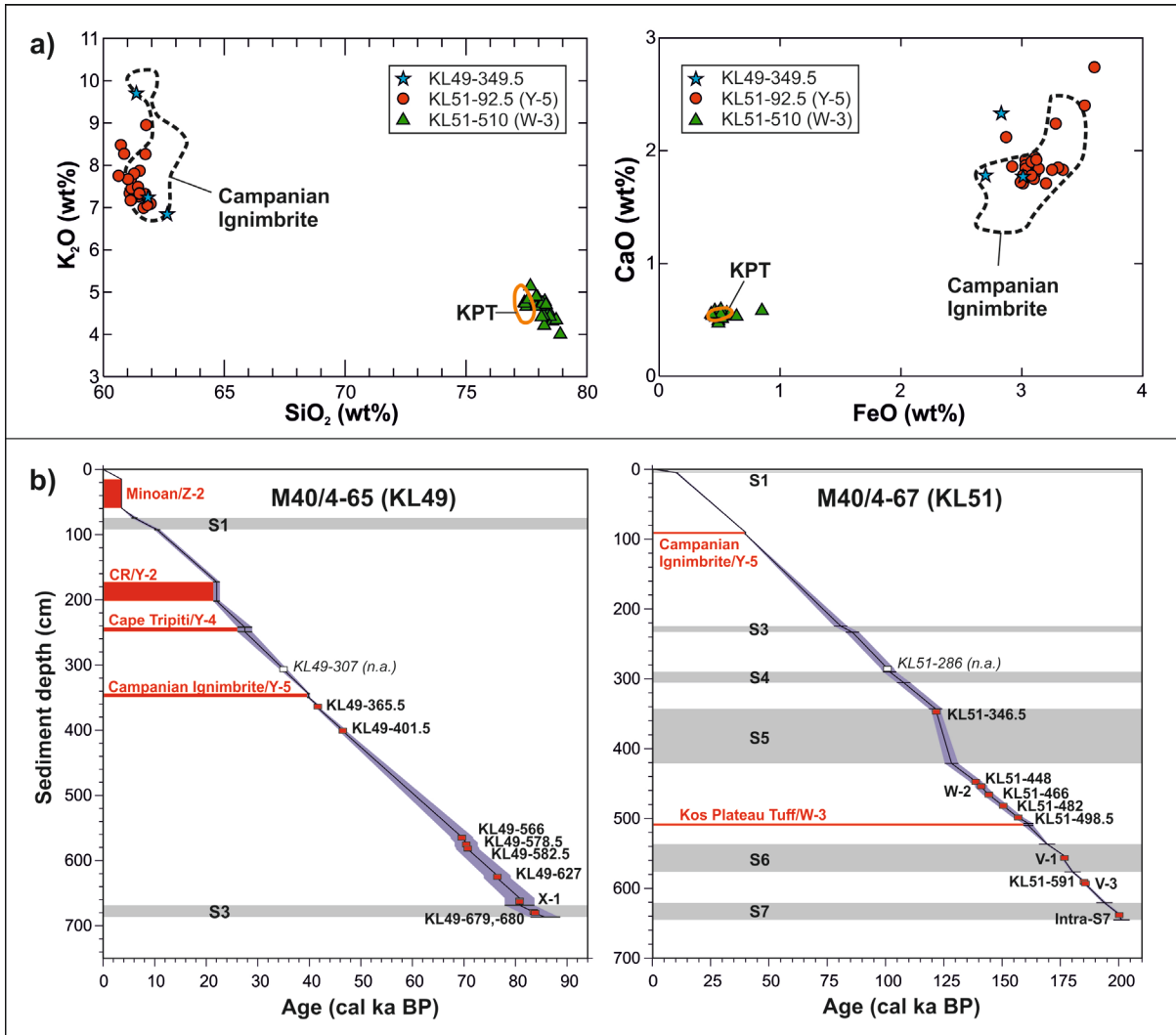
414 **Figure 4:** Bivariate elemental plots of glass composition of the proximal Vourvoulos A fall
415 deposits obtained by different microprobe instruments and analytical setups. Mean EDS glass
416 data from Druitt et al. (1999) is also included for comparison. *(2-column fitting image)*

417

418 **4.4 Chronological constraints of marine Santorini tephras**

419 Correlations of glass geochemical data of proximal Santorini deposits with distal-marine
420 tephra layers have not only allowed for detailed assignments to specific Santorini eruptive
421 events but have also provided new or improved dating of tephras by marine sediment
422 chronologies (Table 2). However, the accuracy and precision of tephra/eruption ages derived
423 this way strongly depends on the reliability and resolution of the sediment core chronologies.
424 The LC21 age model, for example, is based on aligning its high-resolution planktonic
425 foraminiferal oxygen isotope data with the U/Th-dated Soreq cave speleothem $\delta^{18}\text{O}$ record
426 (Bar-Matthews et al., 2000, 2003) and tie-pointing this correlation with radioisotopic ages of
427 two tephra markers, Santorini's Minoan tephra and the Campanian Ignimbrite (Grant et al.,
428 2012). This age model does not only enable precise dating of Santorini tephras (Satow et al.,
429 2015), but also provides improved age estimates of sapropel S1 to S5 boundaries in the
430 Eastern Mediterranean Sea (Grant et al., 2016). These and newly constrained ages of
431 sapropels S6 and S7 from ODP Site 967 (Grant et al., 2017) as well as imported ages of firmly
432 correlated tephra layers, including Z-2/Minoan, Y-2/Cape Riva, Y-4/Cape Tripiti, Y-
433 5/Campanian Ignimbrite and W-3/Kos Plateau Tuff have been used to remodel the previously
434 published chronological frameworks of cores KL49 and KL51 (Keller et al., 2000; Schwarz,
435 2000) (Fig. 5, Supplementary material S4). Linear interpolation of KL49 and KL51
436 chronologies was then applied to constrain eruption age estimates of marine Santorini tephras
437 with 2σ analytical uncertainties (Table 2).

438



439

440 **Figure 5: (a)** Bivariate plots of EPMA glass data of the marine Y-5/Campanian Ignimbrite and
 441 W-3/Kos Plateau Tuff (KPT) tephras occurring in cores KL49 and KL51 (this study; Schwarz,
 442 2000). **(b)** Age-depth model of marine cores KL49 (left) and KL51 (right) with positions of
 443 tephra layers. *(2-column fitting image)*

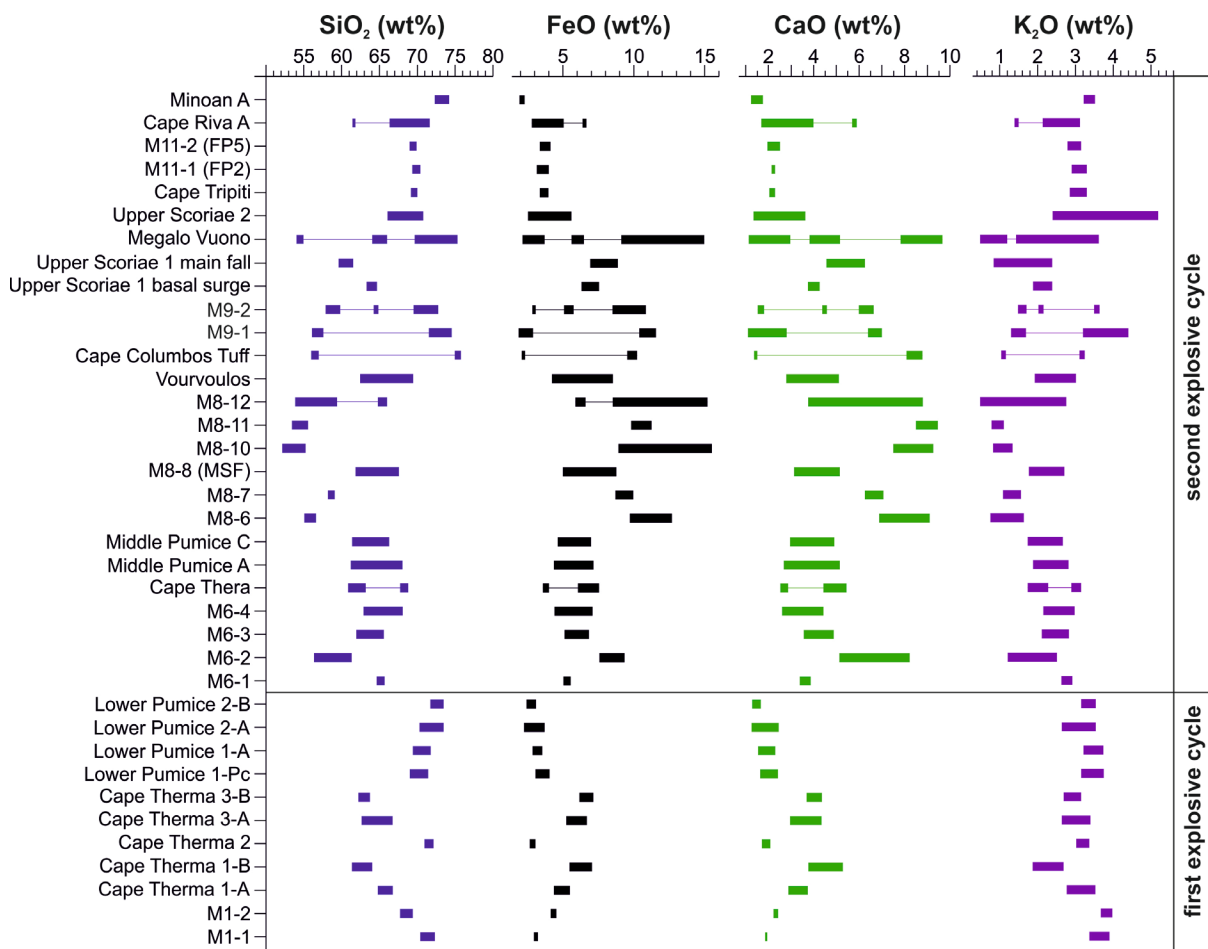
444

445 **5. Glass compositions of proximal tephra deposits**

446 Glass compositions (normalised to 100%) of proximal Santorini tephra fall (and minor flow)
 447 deposits demonstrate a wide range of either basaltic andesitic, andesitic, dacitic or rhyolitic
 448 chemistries which in most cases allow a distinction between individual Plinian and Inter-Plinian
 449 eruptive units (please see detailed descriptions in Supplement material S1). For example,
 450 glass compositions of the major silicic eruptions of Cape Therma 2, Lower Pumice 1 and 2,

451 Cape Riva and Minoan as well as Inter-Plinian deposits M1 are distinguishable from each
 452 other on the basis of slight variations of their SiO₂, FeO, CaO and alkali contents (Figs. 6, S1-
 453 3, S1-8, S1-22 in Supplement material S1). Tephtras of intermediate (andesitic to dacitic) glass
 454 compositions, on the other hand, widely overlap within their major element chemistry and often
 455 do not allow a distinction just on the basis of their major element chemistry alone. This is
 456 especially the case for Plinian and some Inter-Plinian fall deposits of the Middle Tuff Series,
 457 i.e. Cape Thera, Middle Pumice, Vourvoulos, MSF and Upper Scoriae 1 (Figs. 6, S1-11, S1-
 458 14, S1-19). Rhyodacitic tephtras of the M11b Inter-Plinian interval also have very similar major
 459 element glass compositions (Figs. 6, S1-22), indicating a potential correlation between the
 460 different sites in southern Therasia (Cape Tripiti Pumice) and at Oia in northern Thera, which,
 461 however, cannot be specified at this time.

462



463

464 **Figure 6:** Glass elemental variations in SiO₂, FeO, CaO and K₂O (data recalculated to 100
465 wt%, free of volatiles) of proximal tephra deposits listed in stratigraphic order (data from this
466 study only). *(2-column fitting image)*

467

468 Rather peculiar glass compositions have been found in the Cape Columbus (CCT) and Megalo
469 Vouno (MV) deposits. Scoriae of the Cape Columbus Tuff have a dominantly basaltic andesitic
470 glass chemistry and shows an additional very minor rhyolitic component at the top of the
471 proximal deposits (Fig. 6). A similar bimodal composition has been identified in a weathered
472 ash deposit (M9-1) above the Vourvoulos tephra at Phira Steps, suggesting a tentative
473 correlation of the CCT with the M9 Inter-Plinian interval (Fig. S1-14). Megalo Vouno scoriae
474 are characterised by a slightly less silicic chemistry compared to the CCT (Fig. 6). Pumice
475 layers intercalated in the Megalo Vouno cinder cone are bimodal (dacitic and rhyolitic) in
476 composition. The dacitic component closely matches the Upper Scoriae 1 glass composition,
477 while the silicic component is somewhat similar to the unknown rhyolitic one in the CCT (Figs.
478 6, S1-14). The age of the MV cinder cone has been roughly established by K/Ar dating
479 between 54 ± 23 ka and 76 ± 28 ka (Druitt et al., 1999), and stratigraphic relationships
480 suggested by Vespa et al. (2006) restrict it to between the Vourvoulos eruption and the
481 formation of the Skaros Lava Shield (67 ± 9 ka; Fig. 2). This implies the MV deposits were
482 erupted during either the M9 or early M10 Inter-Plinian intervals. Comparison of MV glass
483 chemistries with the M9 Inter-Plinian units show no match (Fig. S1-14), leaving only the
484 possibility of a correlation to the early M10a Inter-Plinian deposits (as proposed by Vespa et
485 al., 2006). Indeed, the geochemical similarity of the intermediate component of the MV
486 deposits to the US1 (Fig. S-14) implies that these two events may have been synchronous; a
487 possibility which is supported further in chapter 6 by the composition of the X-1 tephra layer
488 in deep-sea core KL49.

489

490 ***Please place Table 2 here. (whole A4 page, landscape)***

491

492 **6. Marine tephra correlations**

493 Proximal-marine tephra correlations used a combination of glass chemical matches and
494 information on tephra grain size and chronostratigraphic position in the marine cores that are
495 consistent with the proximal tephra record on Santorini (Druitt et al., 1999). Cores KL49 and
496 KL51 were used to construct a composite tephrostratigraphic framework for the last ~200 kyrs
497 southeast of Santorini. Core KL49 is the closest site to Santorini (30 km) and hence covers
498 the last ~87 kyrs (MIS 1 to MIS 5a) of Santorini activity in greater detail than the distal cores
499 LC21 and KL51. Glass compositions helped to identify 13 visible tephra layers in core KL49
500 that could be assigned to Plinian and Inter-Plinian Santorini eruptive events (Fig. 3, Table 2).

501 Core KL51 derived from the deepest and most distal site 250 km southeast of Santorini. Its
502 sediments are characterised by lower accumulation rates compared to core KL49, and
503 therefore, KL51 covers a larger time interval extending back to ~200 ka (MIS 7 – 1). Ten
504 macroscopic visible tephra layers could be attributed to Santorini Plinian and Inter-Plinian
505 activity based on the same criteria as KL49 tephra (Fig. 3, Table 2).

506 Core LC21 is located in an intermediate position ca. 130 km southeast of Santorini between
507 sites KL49 and KL51 (Fig. 1). Core LC21 has the highest sediment accumulation rates of all
508 three studied marine cores and extends back to ~160 ka (MIS 6 to MIS 1; Grant et al., 2012).
509 Three visible and two cryptotephra layers of Santorini provenance have been identified, three
510 of which have not been assigned to a specific eruptions yet (Satow et al., 2015). The visible
511 Campanian Ignimbrite (39.9 ± 0.1 ka) in all three cores and the Kos Plateau Tuff (161.3 ± 1.1
512 ka; Smith et al., 1996) in KL51 and LC21 were used as chronostratigraphical markers to link
513 the three tephra records and to build a reliable composite tephrostratigraphy (Fig. 3, Table 2).

514 In the following, proximal-marine correlations are discussed in stratigraphic order from the
515 oldest to the youngest deposits.

516

517

518

519 KL51-639.5/Intra-S7 (Cape Therma 3)

520 The oldest marine tephra is a 2.5-cm-thick, fine-grained, dark grey ash layer that is recorded
521 in core KL51 within sapropel S7. Interpolation of the KL51 chronology provided an age
522 estimate for this tephra at 200.2 ± 0.9 ka (Table 2). KL51-639.5 glasses are characterised by
523 a bimodal, andesitic to dacitic glass composition that overlaps with both CTM1 (A,B) and
524 CTM3 (A,B) glass compositions of the new proximal dataset and best agrees with the CTM3-
525 A glass data of Schwarz (2000) (Fig. 7a). A correlation with the CTM3 eruption is also
526 supported by the chronostratigraphic position of the KL51-639.5 tephra at ~ 200 ka, which is
527 in agreement with the K/Ar age of CTM3 underlying Alonaki lavas at 224 ± 5 ka (Druitt et al.,
528 1999); whereas correlation of the KL51-639.5/Intra-S7 tephra layer to the CTM1 eruption is
529 contradicted by the much older age constraint of the proximal CTM1 deposits at ~ 360 ka (Druitt
530 et al., 1999).

531

532 KL51-594/V-3 and KL51-591 (Lower Pumice 1 and M5 Inter-Plinian?)

533 Two tephra layers in core KL51 occur between sapropel S7 and S6 at 594 and 591 cm depth.
534 The lowermost, 2-cm-thick ash layer KL51-594 is the equivalent of the marine V-3 tephra
535 (Hieke et al., 1999) and occurs ~ 16 cm below sapropel S6. It is dated by sapropel interpolation
536 in core KL51 at 185.7 ± 0.7 ka (Table 2). KL51-594/V-3 has a relatively homogenous
537 rhyodacitic glass composition that best matches the major element chemistry of the proximal
538 LP1-A fall deposits of both the new and the Schwarz (2000) dataset (Fig. 7b).

539 The V-3 tephra is closely succeeded by a 1-cm-thick horizon of light grey pumice-lapilli and
540 fine-grained ash. Tephra KL51-591 shows a similar V-3 chemistry except for slightly higher
541 FeO values, resembling the LP1-C (ignimbrite) average glass data by Druitt et al. (1999) (Fig.
542 7b), which suggests potential reworking of the underlying KL51-594/V-3 tephra. However,
543 KL51-591 is deposited 1 cm above the V-3 tephra which indicates a considerable time span
544 of several hundred years in between both layers; therefore, alternatively it could also be
545 derived from a discrete unknown eruptive event within the M5 Inter-Plinian time interval that
546 may have closely followed the LP1 eruption at 185.1 ± 0.7 ka (Fig. 2, Table 2). However, there

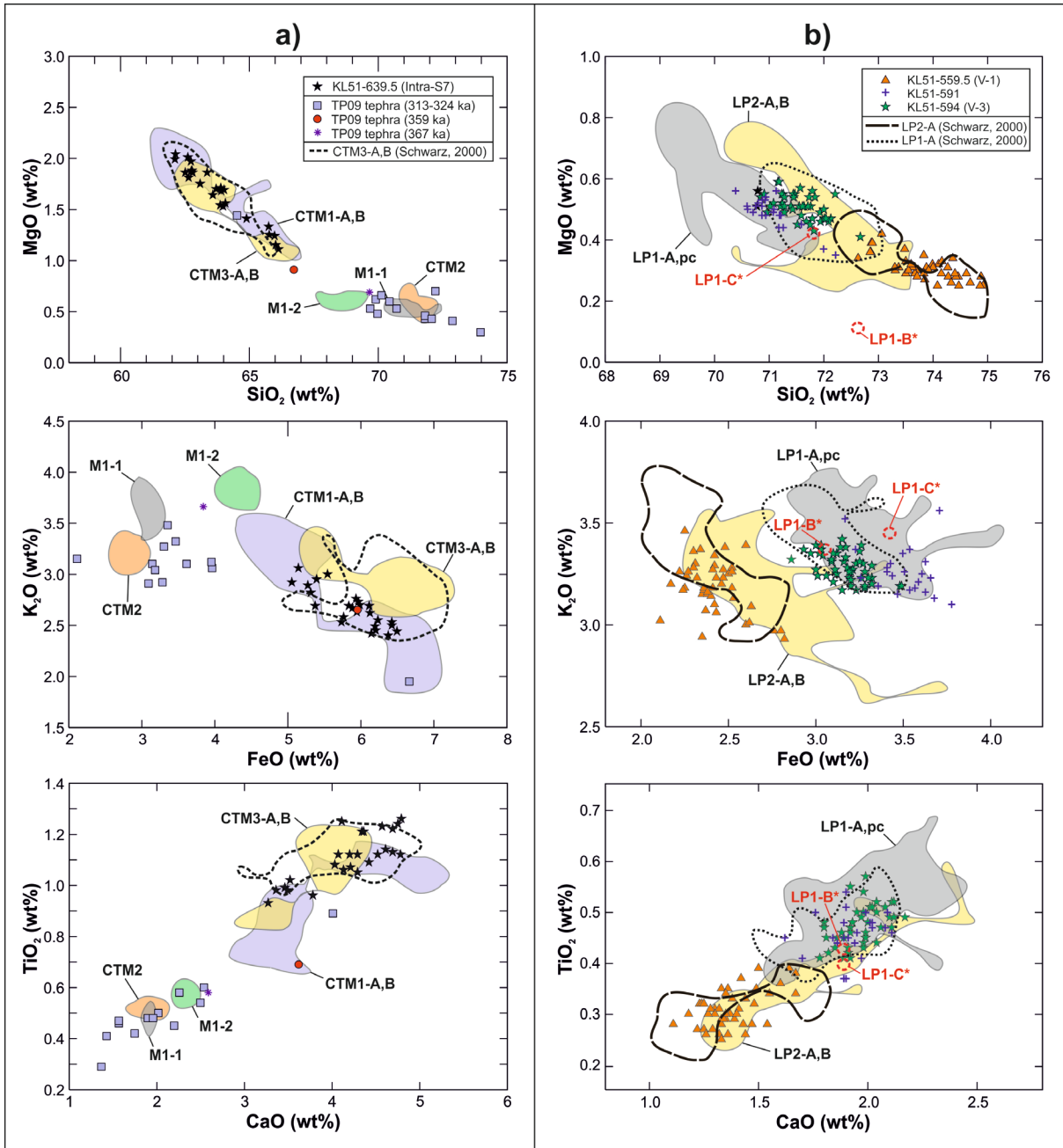
547 is no evidence for volcanic activity between the LP1 and LP2 eruption in the proximal record,
548 hence preventing the collection of glass chemical data for a more detailed comparison with
549 the marine tephra data.

550

551 ***KL51-559.5/V-1 (Lower Pumice 2)***

552 Further up-core in KL51, a 6-cm-thick, fine-grained, light greyish ash layer (KL51-559.5),
553 previously related to the marine V-1 tephra (Hieke et al., 1999), occurs within sapropel S6.
554 KL51-559.5/V-1 has a rhyolitic glass composition that best matches the composition of LP2-A
555 pumices (Fig. 7b). The age of this marine tephra, and thus the LP2 eruption, is interpolated
556 on the basis of the KL51 chronology to 176.7 ± 0.6 ka (Table 2). It is chronostratigraphically
557 in agreement with the $^{40}\text{Ar}/^{39}\text{Ar}$ age of Simandiri lavas at 172 ± 4 ka which overly the proximal
558 LP2 deposits (Druitt et al., 1999), additionally supporting a correlation of the V-1 tephra with
559 the LP2 eruption.

560



561

562 **Figure 7:** Bivariate elemental plots of marine tephra glass data of core KL51 in comparison
 563 with proximal tephra data from **a)** the M1 to CTM3 interval (~360-200 ka) and **b)** the LP1 and
 564 LP2 eruptions (~190-170 ka). Proximal glass data derived from this study; data from Schwarz
 565 (2000) is indicated as black lines, and average EDS glass data from the LP1-B and LP1-C
 566 ignimbritic units are added as red dotted circles (*Druitt et al., 1999). (**2-column fitting image**)

567

568

569

570 KL51-498.5 and LC21-1119 (Cape Thera)

571 Approximately 12 cm above the Kos Plateau Tuff (~161 ka) in core KL51 is a 2-mm-thick, fine
572 ash layer, KL51-498.5, which is dated by sapropel interpolation at 156.9 ± 2.3 ka (Table 2).
573 KL51-498.5 has a heterogeneous andesitic to dacitic chemistry that approximates the
574 composition of both CTA-A and CTA-B (mean) glasses and partly overlaps with MP glass
575 compositions (Fig. 8a). It is stratigraphically positioned below the marine W-2 (KL51-455)
576 which is associated with the Middle Pumice eruption, hence in addition to the glass chemical
577 trend a correlation with the Cape Thera eruption is proposed.

578 In core LC21, a massive, 42-cm-thick Santorini tephra, namely LC21-1119.0, occurs in a
579 similar chronostratigraphic position above the KTP and is dated at 152.6 ± 9.3 ka (Satow et
580 al., 2015). Only a few glass shards have been analysed in LC21-1119.0 ($n=6$), and due to the
581 high microlite content these show a scattered andesitic to dacitic composition that fall into the
582 fields of both the CTA and MP compositions (Fig. 8a). Due to its similar age and chemical
583 composition we propose a tentative correlation of LC21-1119.0 with tephra KL51-498.5 and
584 the CTA eruption.

585

586 KL51-482 and KL51-466 (M7 Inter-Plinian?)

587 In core KL51, two discontinuous ash layers of several mm thickness occur above the KL51-
588 498.5/CTA tephra at 482 cm (150.5 ± 2.4 ka) and 466 cm depth (144.3 ± 2.6 ka). The
589 lowermost KL51-482 tephra has a similar andesitic-dacitic glass composition as KL51-
590 498.5/CTA, while KL51-466 shows a distinct, homogeneous andesitic chemistry (Fig. 8a). Due
591 to their stratigraphical position between the CTA and MP tephtras, KL51-482 and KL51-466
592 most probably relate to M7 Inter-Plinian activity (Table 2), but due to the lack of proximal M7
593 glass data a precise assignment is not possible at this time.

594

595 KL51-455/W-2 (Middle Pumice)

596 In core KL51 between sapropel S6 and S5, a 2.5-cm-thick, relatively coarse lapilli layer occurs
597 that has been previously assigned to the W-2 marine tephra (Hieke et al., 1999). Tephra KL51-

598 455 has a heterogenic dacitic glass composition which matches best the composition of the
599 Middle Pumice A fall deposits (Fig. 8a). It is dated by the KL51 chronology to 141.0 ± 2.6 ka
600 (Table 2).

601

602 ***KL51-448 (M8 Inter-Plinian deposits, MSF?)***

603 Approximately 5.5 cm above the KL51-455/W-2 tephra the coarse-grained (up to 5 mm
604 diameter) and well-sorted (no ash) pumiceous lapilli layer KL51-448 appears. It is ~1 cm thick
605 and has an interpolated age of 138.7 ± 2.7 ka (Table 2). The glass composition of KL51-448
606 is less-silicic than that of KL51-455 and approximates the andesitic-dacitic chemistry of the
607 M8 Main Scoriae Fall (MSF) deposit of Vespa et al. (2006) (Fig. 8b).

608

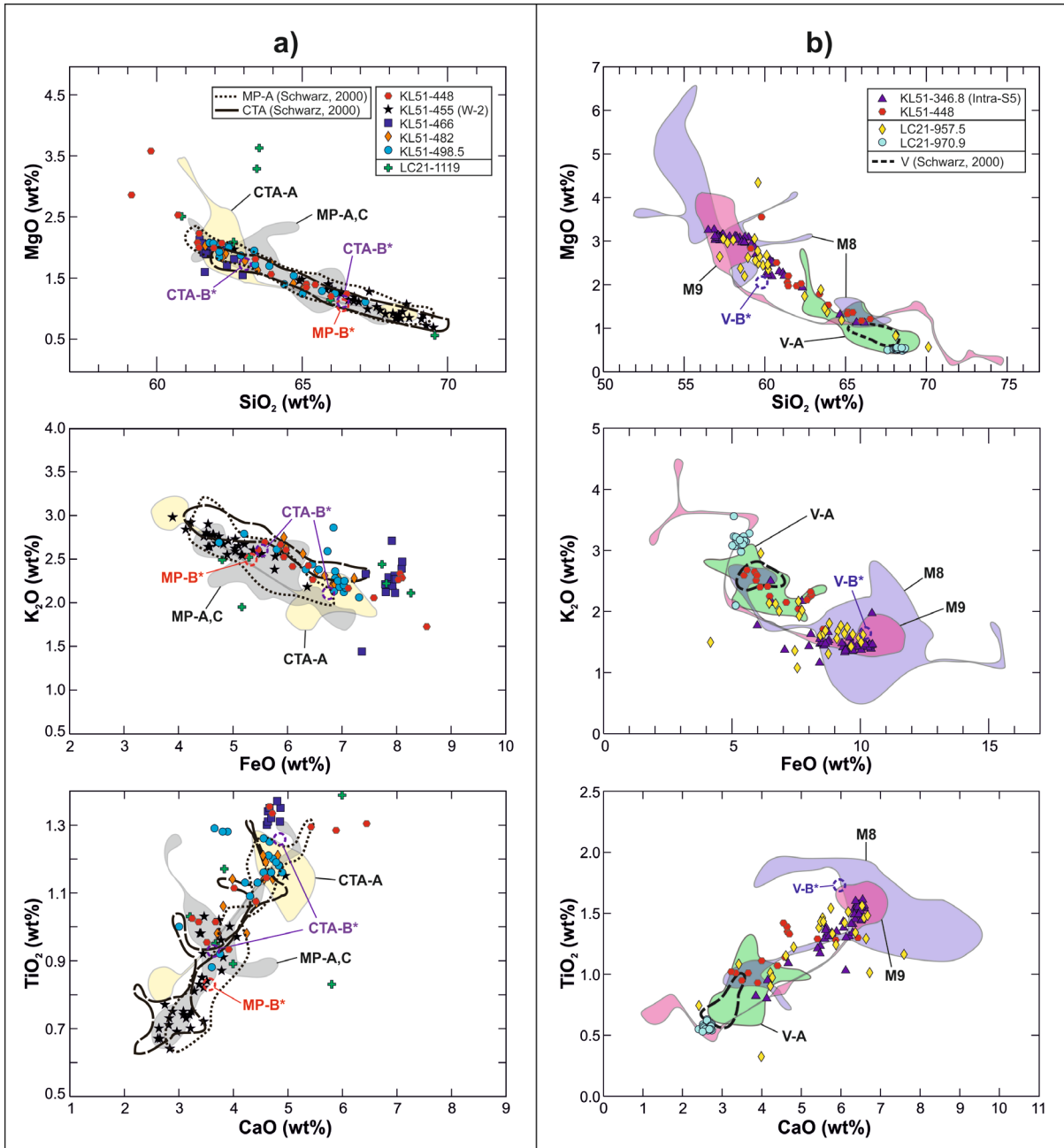
609 ***LC21-970.9 (Vourvoulos), KL51-346.8/Intra-S5 and LC21-957.5 (M9 Inter-Plinian)***

610 The well-laminated top part of sapropel S5 in core KL51 contains a 5-mm-thin, fine-grained
611 ash layer at 346.8 cm depth (Schwarz, 2000; Moller et al., 2012). It is dated by linear
612 interpolation between the upper (121.5 ka) and lower (128.3) sapropel boundary ages at 121.8
613 ± 2.9 ka. KL51-346.8/Intra-S5 is characterised by an andesitic glass composition that mainly
614 overlaps with that of M9-2 Inter-Plinian deposits and partly falls within the fields of the
615 Vourvoulos A fall and Vourvoulos B (co)ignimbritic deposits (Fig. 8b).

616 In core LC21, two tephra layers of Santorini provenance occur within sapropel S5 (Satow
617 et al., 2015). The lower tephra is a visible 1-mm-thick layer, LC21-970.9, which shows a
618 homogeneous dacitic-trachydacitic glass chemistry (Satow et al., 2015) that overlaps with the
619 silicic endmember composition of the Vourvoulos A fall deposits (Fig. 8b). The age of $126.5 \pm$
620 2.9 ka for the LC21-970.9 tephra (Satow et al., 2015) is the first precise age to be derived for
621 the Vourvoulos eruption. The other tephra sample within sapropel S5, LC21-957.5, is taken
622 from a >80 cm glass-shard-rich sediment package above the visible LC21-970.9 tephra
623 (Satow et al., 2015). The base of this shard rich sediment package is separated from the
624 LC21-970.9 tephra by about 10 cm of tephra-free pelagic sediments, implying that it was
625 deposited a significant time after the Vourvoulos eruption. Notably, sample LC21-957.5 has a

626 heterogeneous andesitic to minor dacitic glass composition that fully matches the composition
627 of the visible KL51-346.8/Intra-S5 tephra in core KL51 (Fig. 8b), and hence the two tephra
628 layers are likely to relate to the same eruptive event. Despite the need for further
629 sedimentological investigations of core LC21, we propose a tentative correlation of both the
630 LC21-957.5 and KL51-346.8/Intra-S5 tephra layers to M9 Inter-Plinian deposits. This is
631 supported by their stratigraphic position just above the Vourvoulos tephra (LC21-970.9) and
632 overlapping geochemical composition with the proximal M9 deposits (Figs. 8b and S1-14).
633 M9-2 scoria deposits, with a slightly lower FeO content than the M9-1 weathered ash, are the
634 best match to LC21-957.5 and KL51-346.8/Intra-S5. The interpolated age for this event
635 derives from the KL51 chronology and is defined at 121.8 ± 2.9 ka (Table 2).

636



637

638 **Figure 8:** Bivariate elemental plots of marine tephra glass data of cores KL51 and LC21 in
 639 comparison with proximal tephra data from **a)** the CTA to MP interval (~160-140 ka) and **b)**
 640 the M8, Vourvoulos and M9 eruptions (~140-100 ka). Proximal glass data derived from this
 641 study; data from Schwarz (2000) are indicated as black lines; average EDS glass data from
 642 *Druitt et al. (1999) is added for the CTA-B scoria flow (purple circles) and for the ignimbritic
 643 units MP-B (red circle) and V-B (blue circle). (**2-column fitting image**)

644

645

646 *KL49-680 and KL49-679 (USC1 precursory?)*

647 The oldest tephra layers in core KL49 are two 1–2-mm-thin, fine-grained black ash layers,
648 namely KL49-680 and KL49-679, that both occur within the lower part of sapropel S3. The
649 older tephra KL49-680, dated at 83.8 ± 2.9 ka, is characterised by a dacitic to minor
650 trachydacitic glass composition, which resembles both the composition of the pumice clasts
651 within the basal surge deposits of the USC1 eruption and of the minor dacitic component of
652 the Megalo Vouno pumices (Fig. 9a). The younger KL49-679 tephra (83.5 ± 2.9 ka) has a
653 distinct andesitic composition that approximates more closely the USC1-A main fall
654 composition (Fig. 9a). However, small grain sizes and low thicknesses of both layers in the
655 most proximal core KL49 indicate relatively low-energetic eruption dynamics; hence, we
656 suggest a correlation with fall and flow units that were deposited prior to the main andesitic
657 USC1-A fall tephra, which itself is deposited ~3 cm further upcore in core KL49.

658

659 *KL49-668.5/X-1 (Upper Scoriae 1, Megalo Vouno and Upper Scoriae 2?)*

660 The most prominent tephra in core KL49 is the 8.5-cm-thick, coarse-grained KL49-668.5
661 tephra, which has been previously related to the marine X-1 tephra (Hieke et al., 1999;
662 Schwarz, 2000). It occurs directly on top of sapropel S3 and hence is dated by the KL49 age
663 model at 80.8 ± 2.9 ka (Table 2). Notably, the KL49-668.5/X-1 tephra is subdivided into two
664 sublayers. The lower, 5-cm-thick layer is a black-greyish, coarse-grained (up to 3 cm diameter)
665 scoria lapilli deposit that is characterised by a heterogeneous andesitic-dacitic and basaltic
666 andesitic composition (Fig. 9a). The majority of the intermediate glasses correlate well with
667 the USC1 fall and flow deposits, while the minor mafic components approximate the glass
668 composition of the Megalo Vouno Scoriae (Fig. 9a), hinting at the possibility of a synchronous
669 eruption of this cinder cone at the time of the USC1 eruption.

670 The upper part of the X-1 tephra is a much more fine-grained, black sand layer. Its glasses
671 show a bimodal andesitic and dacitic composition that correlates best with the proximal USC2-
672 A pumice fall and USC2-B scoria flows chemistries (Fig. 9a). Schwarz (2000) reports other X-
673 1 tephra occurrences in more distal marine cores south of Crete where this tephra occurs as

674 a double layer above sapropel S3. Although glass chemical data are not available, the two
675 distinct X-1 layers are a strong indication for two separate, closely-spaced major eruptive
676 events around 70-80 ka. Low sedimentation rates and/or submarine erosional processes at
677 the site of core KL49 could have led to a compression of several tephra events including a
678 large number (n=30) of M10 Inter-Plinian units as described by Vespa et al. (2006), supporting
679 the idea that the X-1 tephra could potentially represent both the USC1 and USC2 eruptions.
680 However, this is rather speculative and requires sedimentological evidence from core KL49.
681 Consequently, other distal marine or terrestrial sediment archives need to be studied to
682 resolve the tephrostratigraphical framework for this particular time interval.

683

684 ***KL49-627, KL49-582.5, KL49-578.5 and KL49-566 (M11a Inter-Plinian)***

685 The KL49-668.5/X-1 tephra is overlain by a succession of four dark, fine-grained ash layers
686 that are dated by interpolation between ~77 ka and 69 ka (Table 2). The lowermost tephra
687 KL49-627 (76.5 ± 2.6 ka) is made up of three closely-spaced, blackish-brown ash lenses in
688 623, 624 and 627 cm depth. Their glass chemistry is identical andesitic and resembles the
689 composition of the proximal USC2-B deposit except for slightly lower MgO and higher TiO₂
690 concentrations (Fig. 9a). The overlying tephra KL49-582.5 (70.7 ± 2.2 ka) is a 2-cm-thick,
691 disperse ash layer with a distinct dacitic glass composition that plots between the USC2-A and
692 USC2-B fields (Fig. 9a). It is closely succeeded by the 6.5-cm-thick, disperse KL49-578.5
693 tephra (70.4 ± 2.2 ka), which is bimodal in composition and overlaps with the andesitic KL49-
694 627 and dacitic KL49-582.5 chemistries (Fig. 9a). It likely represents two compositionally
695 different but synchronous eruptive events. The uppermost layer KL49-566, dated at 69.6 ± 2.1
696 ka, is a 2-cm-thick, dark ash with diffuse lower and upper boundaries. It has a mainly andesitic
697 to minor dacitic glass composition that resembles the andesitic chemistry of the KL49-627 and
698 KL578.5 tephtras except for slightly lower FeO and TiO₂ concentrations (Fig. 9a).

699 Because of the fine-grained nature of tephra components and the glass chemical affinities to
700 the USC2 deposits, the four ash layers in core KL49 may correlate with early M11a Inter-
701 Plinian activity that directly followed the USC2 eruption. Vespa et al. (2006) report six major

702 M11a Inter-Plinian eruption units in the proximal record on Santorini that are characterised by
703 intermediate bulk compositions. Five of these units could be related to the KL49 tephras;
704 however, proximal glass chemistries are still required for potentially confirming and detailing
705 these attributions.

706

707 ***KL49-401.5, KL49-365.5 and KL49-349.5 (M11b Inter-Plinian)***

708 The MIS 3 interval of core KL49 between ~47 ka and 39 ka comprises three visible tephra
709 layers of distinct rhyodacitic glass compositions (Table 2). The lowermost tephra KL49-401.5
710 is a few millimetres thick lens of fine-grained, beige ash that is dated at 46.5 ± 0.7 ka. It has
711 the most evolved glass chemistry with ~67-72 wt% SiO₂ and approximates the composition of
712 both the proximal USC2-A pumice fall and the M11b Inter-Plinian deposits (Fig. 9b). Tephra
713 KL49-365.5 (41.6 ± 0.4 ka) is a 3.5-cm-thick, dark greyish-brown ash layer that has a slightly
714 less silicic glass composition (~67-70 wt% SiO₂) with higher CaO and lower K₂O concentration
715 compared to the preceding KL49-401.5 tephra (Fig. 9b). The uppermost tephra KL49-349.5 is
716 a 5.5-cm-thick, brownish grey, poorly sorted pumice-lapilli and ash deposit that comprises
717 three different glass compositions. The dominant component is dacitic with ~67-69 wt% SiO₂.
718 The second main glass population is a rhyodacite that overlaps with the chemistry of the Y-4
719 tephra that occurs further upcore (Fig. 9b). KL49-349.5 contains also a minor phonolitic-
720 trachytic glass component that correlates well with the Campanian Ignimbrite, hence dating
721 the tephra at 39.9 ± 0.1 ka (Fig. 5). The Campanian Ignimbrite (or marine Y-5 tephra) occurs
722 also as visible layer in cores LC21 (Satow et al., 2015) and KL51 and therefore forms a
723 valuable isochron for linking the three cores (Fig. 3).

724

725 ***KL49-249/Y-4 and LC21-377.5 (Cape Tripiti?)***

726 Tephra KL49-249 occurs in the lower part of the MIS 2 interval in core KL49 and is a ca. 7-
727 cm-thick, dark brownish violet ash layer. It has a homogenous rhyodacitic glass composition
728 that agrees well with the major element chemistry of the marine LC21-377.5/Y-4 cryptotephra
729 in core LC21 (Fig. 9b), where it is dated at 27.5 ± 1.4 ka BP (Satow et al., 2015). Schwarz

730 (2000) originally proposed an assignment of Y-4 to the Upper Scoriae 2 eruption, which was
731 revised by Fabbro et al. (2013) who correlated averaged Y-4 data from core KL49 (Schwarz,
732 2000) and other Aegean Sea cores (Vinci, 1985) with the Cape Tripiti Pumice. The more
733 detailed comparison of the whole KL49-249/Y-4 dataset with new proximal glass data from
734 the Cape Tripiti Pumice, M11-1/FP2, and M11-2/FP5 pyroclastic units confirms an assignment
735 to Santorini M11b activity but does not allow a clear assignment to any of the three units (Fig.
736 9b).

737

738 ***KL49-202/Y-2 (Cape Riva)***

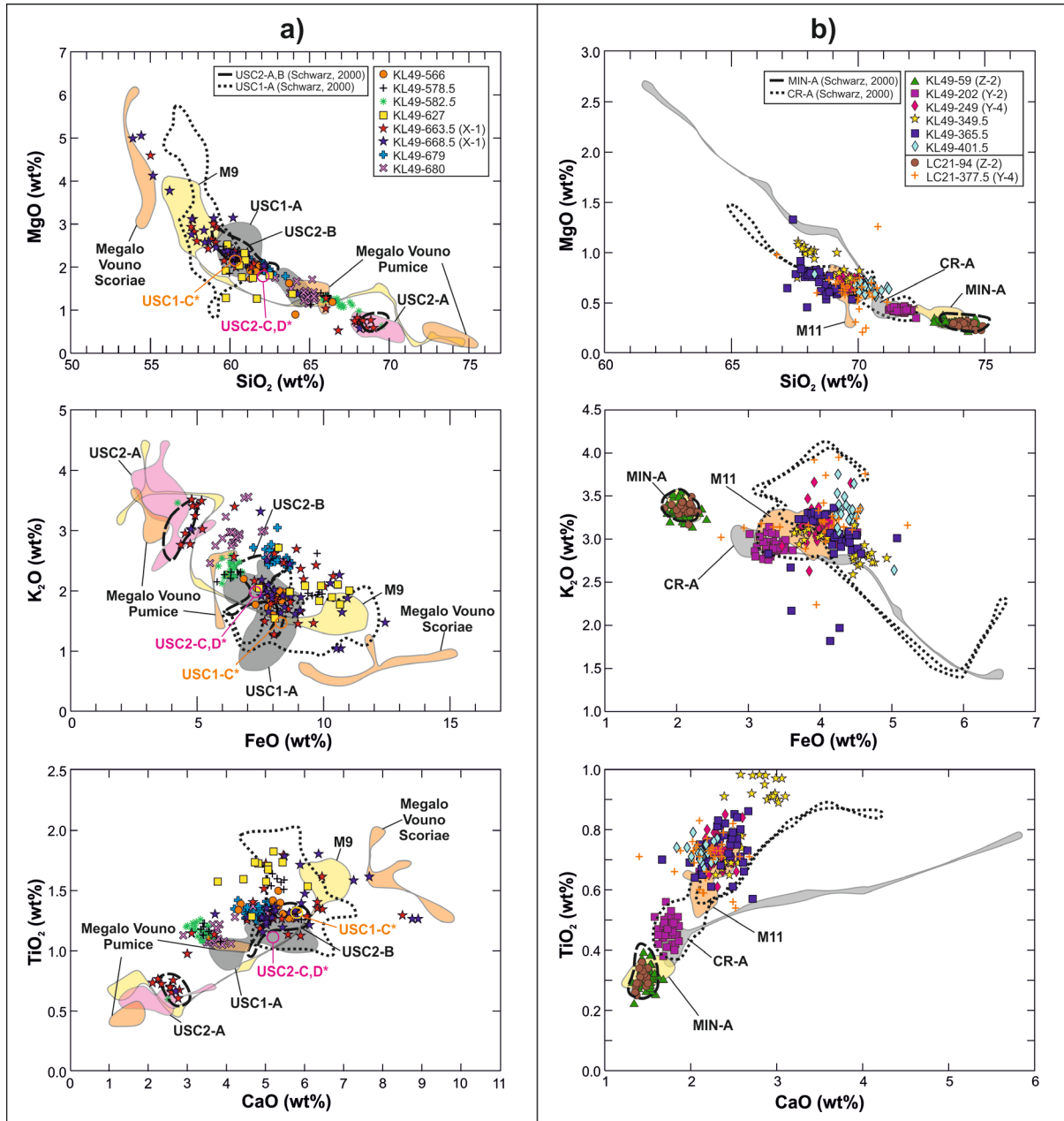
739 The most prominent tephra within the late MIS 2 interval is the ca. 29.5-cm-thick KL49-202
740 layer that is located ca. 80 cm below sapropel S1. It consists of light greyish brown, fine lapilli
741 to sandy stratified material. KL49-202 has a rhyolitic major element chemistry that best
742 matches the composition of both the marine Y-2 tephra and the proximal CR-A fall deposits
743 dated at 22.0 ± 0.6 ka (2σ uncertainty; Bronk Ramsey et al., 2015) (Fig. 9b). This correlation
744 is in agreement with previous interpretations (Schwarz, 2000; Wulf et al., 2002).

745

746 ***KL49-59/Z-2 and LC21-94 (Minoan)***

747 Tephra KL49-59 is positioned above sapropel S1 and represents the youngest and most
748 prominent tephra in core KL49. It is a 44-cm-thick, pale greyish-brown pumice-lapilli (up to 3
749 cm diameter) deposit that is stratified with pale fine lapilli and darker sandy layers. The rhyolitic
750 glass composition clearly assigns KL49-59 to the marine Z-2 and proximal Minoan tephra
751 dated at ~ 3.6 ka (Friedrich et al., 2006) (Fig. 9b). It also correlates with tephra LC21-94 in the
752 more distal core LC21, where it forms a 23-cm thick ash layer (Satow et al., 2015).

753



754

755 **Figure 9:** Bivariate elemental plots of marine tephra glass data of cores KL51 and LC21 in
 756 comparison with proximal tephra data from a) the M9 to USC2 interval (~100-50 ka) and b)
 757 the M11b, Cape Riva and Minoan eruptions (~50-3.6 ka). Proximal glass data derived from
 758 this study; data from Schwarz (2000) are indicated as black lines. Average EDS glass data
 759 from *Druitt et al. (1999) for scoria flows USC1-C (orange circle) and USC2-C,D (pink circles)
 760 have been added for complementing the proximal dataset. (2-column fitting image)

761

762

763 **7. Constraining Santorini eruption ages**

764 **7.1 Ages of marine distal tephras**

765 The different temporal ranges of the three Aegean Sea cores KL49, KL51 and LC21 allowed
766 the preservation of Santorini tephra events from different, partly overlapping time intervals
767 (Table 2). Using mutual prominent tephra markers, such as the Campanian Ignimbrite (all
768 three cores) at 39.9 ± 0.1 ka and the Kos Plateau Tuff (cores KL51 and LC21) at 161.3 ± 2.2
769 ka, facilitates the construction of a continuous distal Santorini tephrostratigraphic framework
770 that covers the last ~200 kyrs (Fig. 3, Table 1).

771 As a result, the newly compiled marine tephrostratigraphy encompasses 27 single eruptive
772 events from Santorini, including ten Plinian and 17 Inter-Plinian eruptions (Table 2). The new
773 age models of cores KL49 and KL51 (this study) as well as the high-resolution LC21
774 chronology (Grant et al., 2012, 2016; Satow et al., 2015) enabled new and/or higher precision
775 dating of previously non- or poorly dated Santorini Plinian events. For example, new eruption
776 dates have been determined for the Vourvoulos (126.5 ± 2.9 ka) and Cape Thera (156.9 ± 2.3
777 ka) eruptions. Furthermore, the new KL49 and KL51 chronologies have updated the age
778 models provided by Keller et al. (2000) and hence now provide higher-precision ages for the
779 Upper Scoriae 1 (80.8 ± 2.9 ka), Middle Pumice (141.0 ± 2.6 ka), Lower Pumice 2 ($176.7 \pm$
780 0.6 ka), Lower Pumice 1 (185.7 ± 0.7 ka), and Cape Therma 3 eruptions (200.2 ± 0.9 ka).

781 Attaining a reliable age estimation of the Upper Scoriae 2 eruption was problematic due the
782 difficulty in unambiguously identifying this tephra as a separate layer in core KL49; its possible
783 stratigraphic position is within the prominent X-1 tephra directly above the USC1 layer. This in
784 addition to rather vague information about its chronostratigraphical position within the X-1
785 double layers in other distal cores (Schwarz, 2000) only allows for constraining a maximum
786 age of the USC2 eruption at 80.8 ± 2.9 ka (the date of the Upper Scoriae 1). In the proximal
787 record, the $^{40}\text{Ar}/^{39}\text{Ar}$ (whole rock) age of the underlying Skaros lavas at 67 ± 9 ka (1σ) provides
788 another maximum age for the USC2 eruption, which lies within the 2σ error range of the marine
789 age estimate. A more reliable $^{40}\text{Ar}/^{39}\text{Ar}$ groundmass age of a lava flow that overlies the USC2
790 deposits at Therasia (48.2 ± 2.4 ka) was derived by Fabbro et al. (2013). This lava is separated

791 from the USC2 deposits by a well-developed palaeosol and represents a minimum age for the
792 USC2 eruption (Fabbro et al., 2013). Direct radioisotopic dating on whole rock material of the
793 USC2 fall deposits has defined its eruption age as either 79 ± 8 ka (1σ , mean K/Ar age) or
794 54.0 ± 3.0 ka (1σ , $^{40}\text{Ar}/^{39}\text{Ar}$) (Druitt et al., 1999). The latter $^{40}\text{Ar}/^{39}\text{Ar}$ date is considered to be
795 the most accurate one at this time as this is a plateau date which should account for any
796 influence from excess argon. It is furthermore also chronostratigraphically in accordance with
797 the date of 67 ± 9 ka (1σ ; Druitt et al., 1999) defined for the underlying Skaros lava shield.
798 However, the KL49 marine record indicates that the USC2 eruption is probably older than 54
799 ka since it closely followed the USC1 event at 80.8 ± 2.9 ka. Only further tephra studies in
800 other distal marine and terrestrial sites as well as new direct dating with modern and more
801 reliable techniques can solve the USC2 dating issue.

802 The marine tephra records also allow for the identification and first dating of Inter-Plinian
803 Santorini activity. The KL49 site nearest to Santorini, for instance, records eruptions preceding
804 USC1 from the M9 interval at 83.8 and 83.5 ± 2.9 ka. KL49 also documents at least ten
805 eruptive events from the M11 Inter-Plinian interval. Those are clustered within two time
806 intervals between 76.5 ± 2.6 ka and 69.6 ± 2.2 ka (M11a; $n=5$) and between 46.5 ± 0.6 ka and
807 27.5 ± 1.4 ka (M11b; $n=5$), respectively.

808 The previously proposed stratigraphic positions of the Megalo Vouno (MV) cinder cone
809 within the early M10a sub-interval (Vespa et al., 2006) is supported by the detection of MV
810 scoriae for the first time at a distal site. Its occurrence within the lower part of the X-1 tephra
811 in core KL49 indicates formation of this cinder cone at around the time of the USC1 eruption
812 (80.8 ± 2.9 ka). The proximal-terrestrial record, where thin dacitic pumice layers matching the
813 USC1 composition are intercalated within the Megalo Vouno scoria, also suggests likely
814 synchronous activity. Furthermore, the tentative assignment of the Cape Columbus Tuff with
815 the proximal M9-1 weathered ash unit directly above the Vourvoulos deposit and the
816 interpolated age estimate of overlying M9-2 scoriae (marine-terrestrial correlations) allow this
817 tuff cone to be constrained to an age between 126.5 ± 2.9 ka and 121.8 ± 2.9 ka. This age is

818 in good agreement with the previously proposed date of the Cape Columbus Tuff during a
819 higher sea-level during MIS 5e that is similar to the present-day sea-level (Druitt et al., 1999).

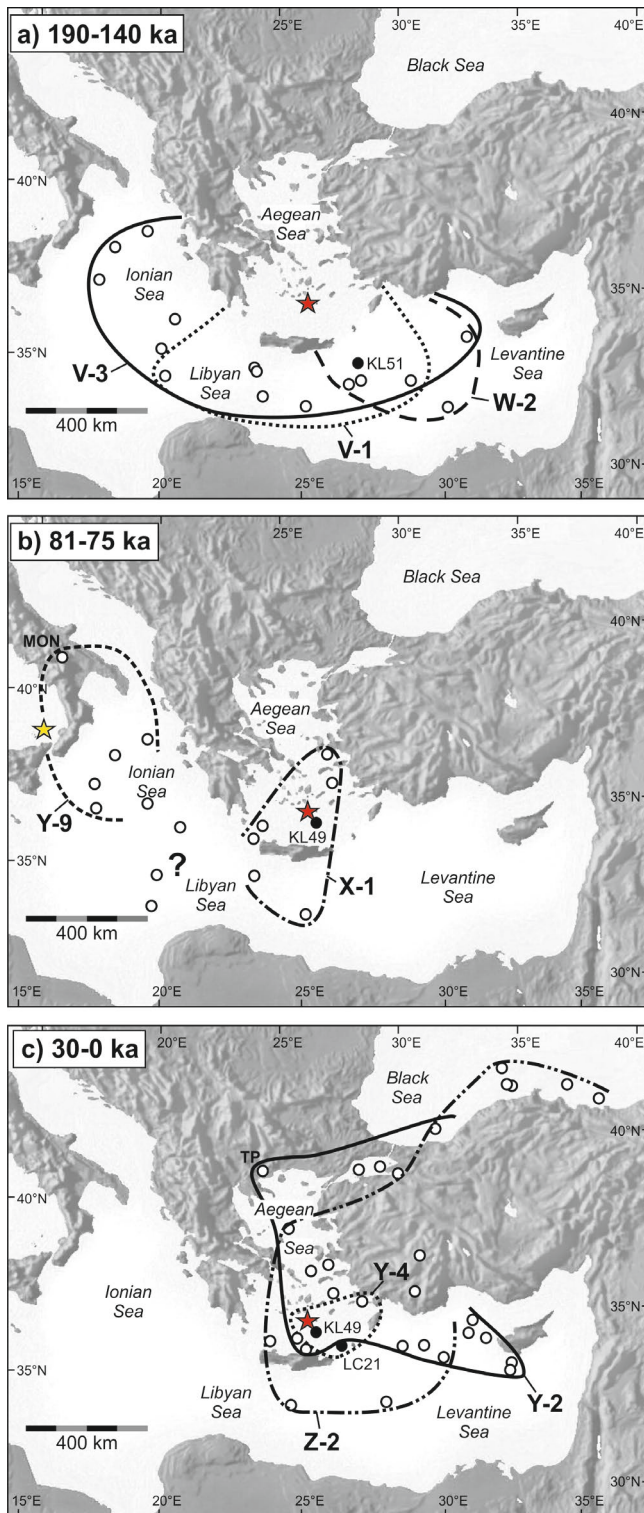
820 Older Inter-Plinian eruptions are documented in core KL51 only. Those include the M8 Main
821 Scoriae Fall (MSF) deposit (Vespa et al., 2006) which occurs stratigraphically above the W-2
822 (Middle Pumice) deposit and is dated at 138.7 ± 2.7 ka. M7 Inter-Plinian activity between the
823 Cape Thera and Middle Pumice eruptions is represented by at least two thin, geochemically
824 slightly distinct fall deposits that are dated at 144.3 ± 2.6 ka and 150.5 ± 2.4 ka, respectively.
825 The oldest Inter-Plinian deposits in the KL51 core potentially relate to the M5 interval and
826 postdate the Lower Pumice 1 tephra to 185.1 ± 0.7 ka (Fig. 3, Table 1).

827

828 **7.2 Palynostratigraphic age constrains of terrestrial distal tephras**

829 The terrestrial peat record of Tenaghi Philippon (TP) in NE Greece (Pross et al., 2015)
830 contains several cryptotephra layers in the MIS 11 to MIS 9 interval that can be connected to
831 the initial phase of the first explosive cycle of Santorini activity (Vakhrameeva et al., 2018,
832 2019) (Fig. 2). The tephrostratigraphic record from TP is used here to complement the marine
833 distal Santorini tephra record and to provide eruption age estimates for the older time interval
834 (>300 ka) of the first explosive cycle by palynostratigraphic dating (Vakhrameeva et al., 2018,
835 2019) (Fig. 2). Accordingly, the oldest Santorini tephra in the TP record occurs within the late
836 MIS 11 interglacial at ~ 367 ka and is correlated with the M1-2 Inter-Plinian eruption
837 (Vakhrameeva et al., 2018). It is followed by the Cape Therma 1 tephra at ~ 359 ka, placing
838 this Plinian eruption at the transition of MIS 11 to MIS 10 (Vakhrameeva et al., 2018). Another
839 eight cryptotephra layers of Santorini provenance form a cluster within the early MIS 9
840 interglacial and are dated palynostratigraphically between ~ 324 ka and 313 ka (Vakhrameeva
841 et al., 2019). The heterogeneous rhyolitic compositions of these tephras approximate the glass
842 composition of both the Cape Therma 2 and M1 tephras (Fig. 5). Based on their position above
843 the CTM1 tephra, these layers are tentatively associated with yet unknown Santorini M2 Inter-
844 Plinian activity (see detailed discussion in Vakhrameeva et al., 2019).

845



846

847 **Figure 10:** Dispersal maps of selected, glass geochemically (EPMA) confirmed Santorini
 848 tephra. Red star indicates the position of Santorini volcano. **(a)** Distribution of MIS 6 tephra
 849 V-3/LP1, V-1/LP2 and W-2/MP; data source: McCoy (1981), Vinci (1985), this study. **(b)**
 850 Distribution of MIS 5a tephra X-1/USC1-USC2? and Y-9/Petrazza; data source: McCoy
 851 (1981), Vinci (1985), Aksu et al. (2008), Wulf et al. (2004), this study. Yellow star represents

852 the location of Stromboli volcano (Aeolian Islands); the distal-terrestrial sites of Lago Grande
853 di Monticchio (MON) is also shown. **(c)** Distribution of MIS 2 and MIS 1 tephras Y-4/Cape
854 Tripiti?, Y-2/CR and Z-2/MIN; the distal-terrestrial site of Tenaghi Philippon (TP) is also
855 included. Selected data from: Federman and Carey (1980), Vinci (1985), Guichard et al.
856 (1993), Eastwood et al. (1999), Aksu et al. (2008), Kwiecien et al. (2008), Sulpizio et al. (2013),
857 Cullen et al. (2014), Satow et al. (2015), Wulf et al. (2002, 2018). **(single column fitting**
858 **image)**

859

860 **8. Santorini tephra dispersal**

861 This study provides new insights into the south-easterly dispersal fan of Santorini tephras in a
862 250-km-long transect represented by the locations of the three marine cores KL49 (30 km
863 distance to Santorini), LC21 (130 km) and KL51 (250 km) (Fig. 1). Although the low number
864 of study sites precludes the generation of detailed isopach maps, tentative information on
865 distribution patterns can be inferred for major tephras in combination with available published
866 data (Table 3).

867 Santorini eruptions that have been long identified at distal marine sites in the Eastern
868 Mediterranean region encompass the tephras V-3/LP1, V-1/LP2, W-2/MP, X-1/USC1-USC2,
869 Y-2/CR, Y-4/Cape Tripiti, and Z-2/MIN (e.g., Keller et al., 1978; Federman and Carey, 1980;
870 Keller, 1981; McCoy, 1981; Vinci, 1985). These tephras have relatively well defined tephra
871 dispersal fans (McCoy, 1981), which, however, are limited to visible tephra findings only. Re-
872 evaluation of these distribution patterns now also includes first cryptotephra findings and
873 terrestrial tephra data (Fig. 10). Findings of older Santorini tephras include mainly the relatively
874 thick MIS 6 layers V-3/LP1 (185.7 ± 0.7 ka), V-1/LP2 (176.7 ± 0.6 ka) and W-2/MP ($141.0 \pm$
875 2.6 ka), which are restricted to core KL51 and to other sediment cores retrieved from deep-
876 sea regions south of Crete, i.e., from the Levantine and Libyan Seas (McCoy, 1981; Vinci,
877 1985) (Fig. 10a). The apparent absence of these tephras north of Santorini is mainly because
878 existing cores from the central and northern Aegean Sea exhibit relatively high sediment
879 accumulation rates and hence do not extend as far back in time. Furthermore, evolving longer

880 (crypto)tephrostratigraphies from distal terrestrial sites north of Santorini (e.g., Tenaghi
881 Philippon; compare Pross et al., 2015; Wulf et al., 2018) still lack information from this
882 particular time interval, and the few data available for the MIS 9 to MIS 11 cryptotephra record
883 are restricted to the Tenaghi Philippon site only (Vakhrameeva et al., 2018, 2019). Sparse
884 information for older Santorini tephras from the proximal-medial record (Druitt et al., 1999)
885 make it particularly difficult to estimate preferred distribution patterns for these tephras.

886 Findings of the V-3/LP1 tephra have been reported in the Libyan and Levantine Basin but
887 also further west in the Ionian Sea (Keller et al., 1978; McCoy, 1981) (Fig. 10a). However,
888 Ionian Sea findings are not yet confirmed by glass geochemical data and hence have to be
889 treated carefully. The W-2/MP tephra (141.0 ± 2.6 ka), on the other hand, has been only
890 identified in the SE Aegean and Levantine Seas, confirming a main southerly to south-easterly
891 dispersal direction of this tephra as proposed by proximal-medial findings (Druitt et al., 1999)
892 (Fig. 10a).

893 The source and dispersal of the marine X-1 tephra (within MIS 5a) have long been
894 controversial. The X-1 tephra has been found in similar stratigraphic positions above sapropel
895 S3 in several cores from the Ionian, Libyan and Aegean Seas (Fig. 10b), and was linked to a
896 mutual source from either Aeolian or Aegean Arc volcanoes (e.g., Federman and Carey, 1980;
897 Keller, 1981; Keller et al., 1978; McCoy, 1981; Vinci, 1985). However, new EPMA glass data
898 have evidenced that there are two different sources involved: The original X-1 tephra, found
899 in Ionian Sea cores a few centimetres above S3 (Kraml, 1997), correlates well with tephra TM-
900 21 in Lago Grande di Monticchio in southern Italy (Wulf et al., 2004). Both tephras have been
901 correlated with the “Petrazza Tuffs” from Stromboli, Aeolian Islands, and dated at 75.3 ± 3.0
902 ka (Kraml, 1997; Wulf et al., 2004). Because of its distinct trachyandesitic to trachydacitic
903 chemistry and its younger age, the former X-1 tephra in Ionian Sea cores has been relabelled
904 as marine Y-9 tephra (Kraml, 1997; Wulf et al., 2004) (Table 3). The former X-1 (double) tephra
905 detected in Aegean Sea cores, in turn, directly overlies S3 at 80.8 ± 2.9 ka and is correlated
906 with the andesitic-dacitic USC1-USC2 eruptions of Santorini (Keller et al., 2000; Schwarz,
907 2000; this study). In this study, X-1 has been only identified in core KL49. Other distal X-1

908 findings include cores from the eastern-central Aegean Sea ca. 200 km NNE of Santorini
909 (Aksu et al., 2008), as well as northwest (Vinci, 1985) and up to 300 km south of Crete (McCoy,
910 1981), the latter confirming a proposed southerly dispersal from the proximal-medial record
911 (Druitt et al., 1999) (Fig. 10b).

912 Dispersal patterns of MIS 2 tephras Y-4, Y-2 and Z-2 are shown in Figure 10c. All three
913 tephras occur in cores KL49 and LC21, with only LC21 lacking the Y-2 tephra. The Y-4/Cape
914 Tripiti? tephra (27.5 ± 1.1 ka) has the most limited distribution within the SE Aegean Sea (Aksu
915 et al., 2008; Satow et al., 2015; this study), probably because of its relative weak eruptive
916 nature. The Y-2/Cape Riva (22.0 ± 0.6 cal ka BP) and Z-2/Minoan tephras (3.6 cal ka BP), on
917 the other hand, show a very widespread dispersal towards the East and North (Y-2) and the
918 Northeast (Z-2) with main occurrences in the Levantine, Aegean and Black Seas (Fig. 10c).

919 Distribution patterns of other major Santorini tephras such as Intra-S7/Cape Therma 3,
920 Cape Thera, and Intra-S5/M9-2 and Vourvoulos are difficult to reconstruct due to their single,
921 first time findings in marine-distal cores (this study) and lack of information from the proximal-
922 medial record. The Intra-S7/CTM3 (200.2 ± 0.9 ka) tephra, for instance, only occurs in core
923 KL51 but is a relative thick layer in that core suggesting a likely south-easterly dispersal. Distal
924 tephra from the Cape Thera (156.9 ± 2.3 ka, MIS 6) and Vourvoulos (126.5 ± 2.9 ka, MIS 5e)
925 eruptions, in turn, are recorded in cores KL51 and LC21, respectively, only as very thin visible
926 layers, indicating either weaker dynamics of these eruptions or a more southerly distribution
927 compared to the Intra-S7/CTM3 tephra.

928 Newly detected distal tephras from minor, Inter-Plinian eruptions, i.e., eruptions from intervals
929 M5, M7, M8, M9, M10, and M11 (Table 2), in the SE sector of Santorini suggest similar
930 southerly to easterly dispersal patterns, however, these need to be tested by further findings.

931

932 ***Please place Table 3 here. (whole A-4 page, landscape)***

933

934

935

936 **9. Concluding remarks and perspectives for future research**

937 This study presents an expanded compilation of glass geochemical data (>1000 analyses) for
938 all Plinian and numerous Inter-Plinian proximal tephra deposits from Santorini and compares
939 this dataset to published and new distal data from SE Aegean Sea cores KL49, KL51 and
940 LC21. As a result of 28 proximal-distal tephra correlations, new or revised interpolated eruption
941 age estimates of seven Plinian (Cape Therma 3, Lower Pumice 1 and 2, Cape Thera, Middle
942 Pumice, Vourvoulos, and Upper Scoriae 1) and 17 Inter-Plinian Santorini events of the past
943 ~200 kyrs could be constrained by interpolation of sapropel and oxygen-isotope-tuned
944 chronologies of these cores. Additionally, both proximal-proximal and proximal-distal
945 correlations provide a more robust chronostratigraphic allocation of the Cape Columbus Tuff
946 and Megalo Vouno cinder cone eruptions possibly within the early M9 Inter-Plinian interval (<
947 121.8 ka) and likely synchronous with the USC1 eruption (80.8 ka), respectively. Results of
948 the tephra studies of marine cores also provide new data on the dispersal of Santorini tephra
949 in a 250 km-transect southeast of Santorini and considerably expands the information
950 available to create isopach maps for the Eastern Mediterranean region.

951 Distal tephrostratigraphic information of the older interval (i.e., >200 ka to ~370 ka) of Santorini
952 activity is provided by the evolving terrestrial (crypto)tephra record of the Tenaghi Philippon
953 peat sequence in NE Greece, located ca. 500 km north of Santorini. To date, the Cape Therma
954 1 tephra and several layers from the M1 and possibly M2 Inter-Plinian interval have been
955 identified and dated by palynostratigraphic constraints (Vakhrameeva et al., 2018, 2019) (Fig.
956 2).

957 The improved ~370 ka Santorini proximal and distal tephrostratigraphies are an important step
958 forward in compiling the Eastern Mediterranean tephra framework, but there is still a need for
959 further research. Future research efforts should include:

- 960 ▪ EPMA glass fingerprinting of additional minor (Inter-Plinian) Santorini tephra deposits:
961 Such analyses are of particular interest for prominent individual units of the M12, M10,
962 M7, M6, M5, and M2 deposits to detail proximal-proximal and proximal-distal tephra
963 correlations.

- 964 ▪ Trace element glass composition of proximal Santorini tephras: Although most
965 Santorini tephras are distinct by their major element glass compositions, there are
966 compositional overlaps which may be resolved by trace element data. Obtaining such
967 data by large-beam (>10 µm) Laser Ablation (LA) ICP-MS, however, may be difficult
968 due to the large amount of microlites in juvenile clasts (e.g., CTA and MP tephras) or
969 the high vesicularity in silicic tephra shards (e.g., LP1 and LP2 tephras). SIMS analysis
970 with spot sizes of 5-10 µm, as already tested on distal Santorini tephra shards in the
971 Tenaghi Philippon record (Vakhrameeva et al., 2018; Wulf et al., 2018), could be a
972 valuable alternative approach.
- 973 ▪ Detailing correlations of distal tephras with specific eruption phases: Distal tephra
974 deposits can derive by fallout from either Plinian or PDC (co-ignimbritic) eruption
975 phases, or from both. Glass chemical data of proximal tephra sub-units from some of
976 the major Santorini eruptions (e.g., CR, USC1, LP2, CTM3) have documented
977 chemical variations between Plinian fall and PDC deposits, and this information was
978 used here to correlate distal marine tephras with distinct eruption phases. Therefore,
979 detailed studies on other proximal Santorini deposits would lead to more
980 comprehensive dataset for understanding eruption dynamics.
- 981 ▪ Radioisotopic dating of Santorini tephras: $^{40}\text{Ar}/^{39}\text{Ar}$ dating of bulk (multi-grain) samples
982 of proximal Santorini tephra may overestimate eruption ages (Druitt et al., 1999). This
983 issue can be overcome by single-grain laser $^{40}\text{Ar}/^{39}\text{Ar}$ analyses, where individual
984 xenocrysts can be identified and removed from the dataset via statistical methods
985 (Kraml, 1997). Another option could be combined U-Th disequilibrium/U-Pb and (U-
986 Th)/He zircon dating of Santorini tephras, a method that has been successfully applied
987 to silicic tephras from e.g. central Anatolia and Ciomadul volcano in Romania (e.g.,
988 Schmitt et al., 2011; Harangi et al., 2015; Danišik et al., 2017). The newly constrained,
989 interpolated ages of marine Santorini tephras (this study) would be a great way to test
990 and identify systematic errors in any of the radioisotopic methods applied to proximal
991 Santorini tephras to provide independent dates.

992
993 ▪ Cryptotephra studies on other marine and terrestrial palaeoenvironmental records:
994 Cryptotephra studies on core LC21 from the southern Aegean Sea (Satow et al., 2015)
995 and in the Tenaghi Philippon peat record from the northern Aegean borderlands
996 (Vakhrameeva et al., 2018, 2019) have demonstrated the great potential to extend the
997 known Santorini tephra dispersal fans. Similar cryptotephra analyses in other long
998 records in the Eastern Mediterranean region (e.g., SE Balkan Peninsula, Asia Minor,
999 Black Sea and Dead Sea) would greatly enhance this knowledge and additionally
1000 provide valuable time markers for these records.

1001

1002 **Acknowledgements**

1003 Special thanks go to Michael Schwarz who did an enormous effort to obtain glass chemical
1004 data of tephtras from marine cores KL49 and KL51 for a Diploma thesis and who kindly
1005 provided his dataset for this study. We thank Sean Whitley (Keele University) for collecting the
1006 Cape Tripiti pumice sample used in this study and Monika Doubrava (Heidelberg University)
1007 for helping with SAN15 tephra thin-section preparation. We furthermore acknowledge John
1008 Spratt (Natural History Museum, London) for his kind assistance in the EPMA analysis of
1009 samples SAN16 and SAN17, and Ian Gill (Kingston University) for his skilled mounting and
1010 polishing of these samples. Funding for Santorini fieldwork was supported partially by
1011 Heidelberg University. JK, MK, AK, JP and PV acknowledge financial support by the Deutsche
1012 Forschungsgemeinschaft (DFG; grants KE136/35, KE 136/37, KO4960/3 and PR651/19).
1013 Finally, we would like to thank Tim Druitt and Biagio Giaccio for their mindful and constructive
1014 comments and suggestions for improving an earlier version of this manuscript.

1015

1016 **Appendix A: Supplementary data**

1017 **Supplementary material S1:** Sampling sites and detailed chemical descriptions of proximal
1018 tephra deposits on Santorini.

1019 **Supplementary material S2:** EPMA glass data of proximal tephra deposits from Santorini
1020 analysed in this study.

1021 **Supplementary material S3:** EPMA glass data of marine tephras from cores KL49 and KL51
1022 (Schwarz, 2000), and LC21 (Satow et al., 2015).

1023 **Supplementary material S4:** Age-depth models for marine cores KL49 and KL51.

1024

1025 **References**

1026 Abu-Zied, R.H., Rohling, E.J., Jorissen, F.J., Fontanier, C., Casford, J.S.L. and Cooke, M.,
1027 2008. Benthic foraminiferal response to changes in bottom water oxygenation and
1028 organic carbon flux in the eastern Mediterranean during LGM to recent times. *Marine*
1029 *Micropaleontology*, 67: 46-68.

1030 Aksu, A.E., Jenner, G., Hiscott, R.N. and Isler, E.B., 2008. Occurrence, stratigraphy and
1031 geochemistry of Late Quaternary tephra layers in the Aegean Sea and the Marmara
1032 Sea. *Marine Geology*, 252: 174-192.

1033 Albert, P.G., Tomlinson, E.L., Lane, C.S., Wulf, S., Smith, V.C., Coltelli, M., Keller, J., Lo
1034 Castro, D., Manning, C.J., Müller, W. and Menzies, M.A., 2013. Late glacial explosive
1035 activity on Mount Etna: Implications for proximal-distal tephra correlations and the
1036 synchronisation of Mediterranean archives. *Journal of Volcanology and Geothermal*
1037 *Research*, 265: 9-26.

1038 Albert, P.G., Hardiman, M., Keller, J., Tomlinson, E.L., Smith, V.C., Bourne, A.J., Wulf, S.,
1039 Zanchetta, G., Sulpizio, R., Müller, U.C., Pross, J., Ottolini, L., Matthews, I.P., Blockley,
1040 S.P.E. and Menzies, M.A., 2015. Revisiting the Y-3 tephrostratigraphic marker: a new
1041 diagnostic glass geochemistry, age estimate, and details on its climatostratigraphical
1042 context. *Quaternary Science Reviews*, 118: 105-121.

1043 Albert, P., Tomlinson, E.L., Smith, V.C., Di Traglia, F., Pistolesi, M., Morris, A., Donato, P., De
1044 Rosa, R., Sulpizio, R., Keller, J., Rosi, M. and Menzies, M., 2017. Glass geochemistry

- 1045 of pyroclastic deposits from the Aeolian Islands in the last 50 ka: A proximal database
1046 for tephrochronology. *Journal of Volcanology and Geothermal Research*, 336: 81-107.
- 1047 Angelier, J., Lyberis, N., Le Pichon, X., Barrier, E. and Huchon, P., 1982. The tectonic
1048 development of the Hellenic arc and the Sea of Crete: a synthesis. *Tectonophysics*,
1049 86: 159-196.
- 1050 Antonopoulos, J., 1992. The Great Minoan eruption of Thera volcano and the ensuing
1051 Tsunami in the Greek Archipelago. *Natural Hazards*, 5: 153-168.
- 1052 Bar-Matthews, M., Ayalon, A., Gilmour, M., Matthews, A. and Hawkesworth, C.J., 2003. Sea-
1053 land oxygen isotopic relationships from planktonic foraminifera and speleothems in the
1054 Eastern Mediterranean region and their implication for paleorainfall during interglacial
1055 intervals. *Geochimica et Cosmochimica Acta*, 67(17): 3181-3199.
- 1056 Bar-Matthews, M., Ayalon, A. and Kaufmann, A., 2000. Timing and hydrological conditions of
1057 Sapropel events in the Eastern Mediterranean, as evident from speleothems, Soreq
1058 cave, Israel. *Chemical Geology*, 169: 145-156.
- 1059 Bond, A. and Sparks, R.S.J., 1976. The Minoan eruption of Santorini, Greece. *Journal of the*
1060 *Geological Society of London* 132: 1-16.
- 1061 Bronk Ramsey, C., Albert, P.G., Blockley, S.P.E., Hardiman, M., Housley, R.A., Lane, C.S.,
1062 Lee, S., Matthews, I.P., Smith, V.C. and Lowe, J.J., 2015. Improved age estimates for
1063 key Late Quaternary European tephra horizons in the RESET lattice. *Quaternary*
1064 *Science Reviews*, 118: 18-32.
- 1065 Bruins, H.J., MacGillivray, A., Synolakis, C.E., Benjamini, C., Keller, J., Kisch, H.J., Klügel, A.,
1066 and van der Plicht, J., 2008. Geoarchaeological tsunami deposits at Palaikastro
1067 (Crete) and the Late Minoan IA eruption of Santorini. *Journal of Archaeological*
1068 *Science*, 35(1): 191-212.
- 1069 Bruins, H.J., Keller, J., Klügel, A., Kisch, H.J., Kutra, I. and van den Plicht, J., 2019. Tephra in
1070 caves: Distal deposits of the Minoan Santorini eruption and the Campanian super-
1071 eruption. *Quaternary International*, 499: 135-147.

- 1072 Çagatay, M.N., Wulf, S., Sancar, Ü., Özmaral, A., Vidal, L., Henry, P., Appelt, O. and
1073 Gasperini, L., 2015. The tephra record from the Sea of Marmara for the last ca. 70 ka
1074 and its palaeoceanographic implications. *Marine Geology*, 361: 96-110.
- 1075 Casford, J.S.L., Rohling, E.J., Abu-Zied, R.H., Jorissen, F.J., Leng, M. and Thomson, J., 2003.
1076 A dynamic concept for eastern Mediterranean circulation and oxygenation during
1077 sapropel formation. *Palaeogeography, Palaeoclimatology, Palaeoecology*, 190: 103-
1078 119.
- 1079 Cullen, V.L., Smith, V.C. and Arz, H.W., 2014. The detailed tephrostratigraphy of a core from
1080 the south-east Black sea spanning the last ~60 ka. *Journal of Quaternary Science*,
1081 29(7): 675-690.
- 1082 Danišík, M., Schmitt, A.K., Stockli, D.F., Lovera, O.M., Dunkl, I. and Evans, N.J., 2017.
1083 Application of combined U-Th-disequilibrium/U-Pb and (U-Th)/He zircon dating to
1084 tephrochronology. *Quaternary Geochronology*, 40: 23-32.
- 1085 Davies, S.M., Abbott, P.M., Meara, R.H., Pearce, N.J.G., Austin, W.E.N., Chapman, M.R.,
1086 Svensson, A., Bigler, M., Rasmussen, T.L., Rasmussen, S.O. and Farmer, E.J., 2014.
1087 A North Atlantic tephrostratigraphical framework for 130-60 ka b2k: new tephra
1088 discoveries, marine-based correlations, and future challenges. *Quaternary Science*
1089 *Reviews*, 106: 101-121.
- 1090 De Rijk, A., Hayes, A. and Rohling, E.J., 1999. Eastern Mediterranean sapropel S1 interruption
1091 and expression of the climatic deterioration around 7 ka BP. *Marine Geology*, 153:
1092 337-343.
- 1093 Devine, J.D., Gardner, J.E., Brack, H.P., Layne, G.D. and Rutherford, M.J., 1995. Comparison
1094 of microanalytical methods for estimation of H₂O-contents of silicic volcanic glasses.
1095 *American Mineralogist*, 80: 319-328.
- 1096 Doulas, C. and Papazoglou, L., 1980. Santorini tephra from Rhodes. *Nature*, 287: 322-324.
- 1097 Druitt, T.H., 1985. Vent evolution and lag breccia formation during the Cape Riva eruption of
1098 Santorini, Greece. *Journal of Geology*, 93: 439-454.

- 1099 Druitt, T.H., Edwards, L., Mellors, R.M., Pyle, D.M., Sparks, R.S.J., Lanphere, M., Davies, M.
1100 and Barriero, B., 1999. Santorini Volcano. Geological Society Special Publications, 19.
1101 Geological Society, London, 165 pp.
- 1102 Druitt, T.H., Mellors, R.A., Pyle, D.M. and Sparks, R.S.J., 1989. Explosive volcanism on
1103 Santorini, Greece. Geological Magazine, 126(2): 95-126.
- 1104 Druitt, T.H. and Sparks, R.S.J., 1982. A proximal ignimbrite breccia facies on Santorini,
1105 Greece. Journal of Volcanology and Geothermal Research, 13: 147-171.
- 1106 Druitt, T.H., Francalanci, L. and Fabbro, G., 2015. Field guide to Santorini volcano. MeMoVolc
1107 short course, Santorini: pp. 56
- 1108 Eastwood, W.J., Pearce, N.J.G., Westgate, J.A., Perkins, W.T., Lamb, H.F. and Roberts, N.,
1109 1999. Geochemistry of Santorini tephra in lake sediments from Southwest Turkey.
1110 Global and Planetary Change, 21: 17-29.
- 1111 Edwards, L., 1994. Magma cyclicity and isotopic variation on Santorini volcano, Aegean Sea,
1112 Greece. PhD Thesis, University of Bristol, 372 pp.
- 1113 Fabbro, G.N., Druitt, T.H. and Scaillet, S., 2013. Evolution of the crustal magma plumbing
1114 system during the build-up to the 22-ka caldera-forming eruption of Santorini (Greece).
1115 Bulletin of Volcanology, 75: 767.
- 1116 Federman, A.N. and Carey, S.N., 1980. Electron microprobe correlation of tephra layers from
1117 Eastern Mediterranean abyssal sediments and the island of Santorini. Quaternary
1118 Research, 13: 160-171.
- 1119 Fletcher, W.J., Müller, U., Koutsodendris, A., Christanis, K. and Pross, J., 2013. A centennial-
1120 scale record of vegetation and climate variability from 312 to 240 ka (Marine Isotope
1121 Stages 9c-a, 8 and 7e) from Tenaghi Philippon, NE Greece. Quaternary Science
1122 Reviews, 78: 108-125.
- 1123 Fouqué, F., 1879. Santorin et ses éruptions. Masson, Paris.
- 1124 Friedrich, W.L., 2000. Fire in the Sea. The Santorini volcano: natural history and the legend of
1125 Atlantis. Translated by A.R. McBirney. Cambridge: Cambridge University Press.

- 1126 Friedrich, W.L., Kromer, B., Friedrich, M., Heinemeier, J., Pfeiffer, T. and Talamo, S., 2006.
1127 Santorini eruption radiocarbon dated to 1627–1600 B.C. *Science*, 312: 548.
- 1128 Fytikas, M., Kolios, N. and Vougioukalakis, G., 1990. Post-Minoan volcanic activity of the
1129 Santorini volcano. Volcanic hazard and risk, forecasting possibilities. In: D.A. Hardy
1130 (Editor), *Thera and the Aegean World III*. The Thera Foundation, London, pp. 183-198.
- 1131 Gertisser, R., Preece, K. and Keller, J., 2009. The Plinian Lower Pumice 2 eruption, Santorini,
1132 Greece: Magma evolution and volatile behaviour. *Journal of Volcanology and*
1133 *Geothermal Research*, 186: 387-406.
- 1134 Giaccio, B., Nomade, S., Wulf, S., Isaia, R., Sottili, G., Cayuoto, G., Galli, P., Messina, P.,
1135 Sposato, A., Sulpizio, R. and Zanchetta, G., 2012. The late MIS 5 Mediterranean
1136 tephra markers: a reappraisal from peninsular Italy terrestrial records. *Quaternary*
1137 *Science Reviews*, 56: 31-45.
- 1138 Giaccio, B., Niespolo, E.M., Pereira, A., Nomade, S., Renne, P.R., Albert, P.G., Arienzo, I.,
1139 Regattieri, E., Wagner, B., Zanchetta, G., Gaeta, M., Galli, P., Mannella, G., Peronace,
1140 E., Sottili, G., Florindo, F., Leicher, N., Marra, F. and Tomlinson, E.L., 2017a. First
1141 integrated tephrochronological record for the last ~190 kyr from the Fucino Quaternary
1142 lacustrine succession, central Italy. *Quaternary Science Reviews*, 158: 211-234.
- 1143 Giaccio, B., Hajdas, I., Isaia, R., Deino, A. and Nomade, S., 2017b. High-precision ^{14}C and
1144 $^{40}\text{Ar}/^{39}\text{Ar}$ dating of the Campanian Ignimbrite (Y-5) reconciles the time-scale of climatic
1145 cultural processes at 40 ka. *Scientific Reports*, 7: 45940.
- 1146 Grant, K.M., Grimm, R., Mikolajewicz, U., Marino, G., Ziegler, M. and Rohling, E.J., 2016. The
1147 timing of Mediterranean sapropel deposition relative to insolation, sea-level and
1148 African monsoon changes. *Quaternary Science Reviews*, 140: 125-141.
- 1149 Grant, K.M., Rohling, E.J., Bar-Matthews, M., Ayalon, A., Medina-Elizalde, M., Bronk Ramsey,
1150 C., Satow, C. and Roberts, A.P., 2012. Rapid coupling between ice volume and polar
1151 temperature over the past 150,000 years. *Nature*, 491: 744-747.

- 1152 Grant, K.M., Rohling, E.J., Westerhold, T., Zabel, M., Heslop, D., Konijnendijk, T. and Lourens,
1153 L., 2017. A 3 million year index for North African humidity/aridity and the implication
1154 of potential pan-African Humid periods. *Quaternary Science Reviews*, 171: 100-118.
- 1155 Gudmundsdóttir, E.R., Larsen, G., Björck, S., Ingólfsson, Ó. and Striberger, J., 2016. A new
1156 high-resolution Holocene tephra stratigraphy in eastern Iceland: Improving the
1157 Icelandic and North Atlantic tephrochronology. *Quaternary Science Reviews*, 150:
1158 234-249.
- 1159 Guichard, F., Carey, S., Arthur, M.A., Sigurdsson, H. and Arnold, M., 1993. Tephra from the
1160 Minoan eruption of Santorini in sediments of the Black Sea. *Nature*, 363: 610-612.
- 1161 Harangi, S., Lukács, R., Schmitt, A.K., Dunkl, I., Molnár, K., Kiss, B., Seghedi, I., Novothny,
1162 Á. and Molnár, M., 2015. Constraints on the timing of Quaternary volcanism and
1163 duration of magma residence at Ciomadul volcano, east-central Europe, from
1164 combined U-Th/He and U-Th zircon geochronology. *Journal of Volcanology and
1165 Geothermal Research*, 301: 66-80.
- 1166 Hayes, A., Rohling, E.J., De Rijk, A., Kroon, D. and Zachariesse, W.J., 1999. Mediterranean
1167 planktonic foraminiferal faunas during the Last Glacial cycle. *Marine Geology*, 153:
1168 239-252.
- 1169 Hieke, W., Hemleben, C., Linke, P., Türkay, M. and Weikert, H., 1999. *Mittelmeer 1998/99,*
1170 *Cruise No. 40, 28 October 1997 – 10 February 1998, Universität Hamburg.*
- 1171 Hunt, J.B. and Hill, P.G., 1996. An inter-laboratory comparison of the electron probe
1172 microanalysis of glass geochemistry. *Quaternary International*, 34-36: 229-241.
- 1173 Insinga, D.D., Tamburrino, S., Lirer, F., Vezzoli, L., Barra, M., De Lange, G.J., Tiepolo, M.,
1174 Vallefucio, M., Mazzola, S. and Sprovieri, M., 2014. Tephrochronology of the
1175 astronomically-tuned KC01B deep-sea core, Ionian Sea: insights into the explosive
1176 activity of the Central Mediterranean area during the last 200 ka. *Quaternary Science
1177 Reviews*, 85: 63-84.
- 1178 Jochum, K.P., Stoll, B., Herwig, K., Willbold, M., Hofmann, A.W., et al., 2006. MPI-DING
1179 reference glasses for in situ microanalysis: New reference values for element

- 1180 concentrations and isotope ratios. *Chemistry, Geophysics, Geosystems*, 7(2):
1181 Q02008.
- 1182 Keller, J., 1981. Quaternary tephrochronology in the Mediterranean region. In: S. Self and
1183 R.S.J. Sparks (Editors), *Tephra Studies*. Reidel, Dordrecht, pp. 227-244.
- 1184 Keller, J., Kraml, M. and Schwarz, M., 2000. Dating major volcanic paroxysms within the deep-
1185 sea record: the example of the Thera Formation, Santorini, Greece, IAVCEI General
1186 Assembly, Bali, Indonesia, pp. 16.
- 1187 Keller, J. and Ninkovich, D., 1972. Tephra-Lagen in der Ägäis. *Z. Deutsch. Geol. Ges.*, 123:
1188 579-587.
- 1189 Keller, J., Ryan, W.B.F., Ninkovich, D. and Altherr, R., 1978. Explosive volcanic activity in the
1190 Mediterranean over the past 200,000 yr as recorded in deep-sea sediments.
1191 *Geological Society of America Bulletin*, 89: 591-604.
- 1192 Keller, J., Gertisser, R., Reusser, E. and Dietrich, V., 2014. Pumice deposits of the Santorini
1193 Lower Pumice 2 eruption on Anafi island, Greece: Indications for a Plinian event of
1194 exceptional magnitude. *Journal of Volcanology and Geothermal Research*, 278-279:
1195 120-128.
- 1196 Konijnendijk, T.Y.M., Ziegler, M. and Lourens, L.J., 2015. On the timing and forcing
1197 mechanisms of late Pleistocene glacial terminations: Insights from a new high-
1198 resolution benthic stable oxygen isotope record of the eastern Mediterranean.
1199 *Quaternary Science Reviews*, 129: 308-320.
- 1200 Kraml, M., 1997. Laser-⁴⁰Ar/³⁹Ar-Datierungen an distalen marinen Tephren des jung-quartären
1201 mediterranen Vulkanismus (Ionisches Meer, METEOR-Fahrt 25/4). PhD Thesis,
1202 Albert-Ludwigs-Universität Freiburg, 216 pp.
- 1203 Kuehn, S.C., Froese, D.G., Shane, P.A.R. and INTAV Intercomparison Participants, 2011.
1204 The INTAV intercomparison of electron-beam microanalysis of glass by
1205 tephrochronology laboratories: Results and recommendations. *Quaternary*
1206 *International*, 246: 19-47.

- 1207 Kwiecien, O., Arz, H.W., Lamy, F., Wulf, S., Bahr, A., Röhl, U. and Haug, G.H., 2008.
1208 Estimated reservoir ages of the Black Sea since the Last Glacial. *Radiocarbon*, 50(1):
1209 1-20.
- 1210 Lane, C.S., Brauer, A., Blockley, S.P.E. and Dulski, P., 2013. Volcanic ash reveals time-
1211 transgressive abrupt climate change during the Younger Dryas. *Geology*, 41: 1251-
1212 1254.
- 1213 Larsen, G. and Eiriksson, J., 2008. Late Quaternary terrestrial tephrochronology of Iceland -
1214 frequency of explosive eruptions, type and volume of tephra deposits. *Journal of*
1215 *Quaternary Science*, 23(2): 109-120.
- 1216 Laurenzi, M.A. and Villa, I.M., 1987. $^{40}\text{Ar}/^{39}\text{Ar}$ chronostratigraphy of Vico ignimbrites. *Periodico*
1217 *di Mineralogia*, 56: 285-293.
- 1218 Lawson, I.T., Swindles, G.T., Plunkett, G. and Greenberg, D., 2012. The spatial distribution of
1219 Holocene cryptotephra in north-west Europe since 7 ka: implications for
1220 understanding ash fall events from Icelandic eruptions. *Quaternary Science Reviews*,
1221 41: 57-66.
- 1222 Li, X., Bock, G., Vafidis, A., Kind, R., Harjes, H.P., Hanka, W., Wylegalla, K., van der Meijde,
1223 M. and Yuan, X., 2003. Receiver function study of the Hellenic subduction zone:
1224 imaging crustal thickness variations and the oceanic Moho of the descending African
1225 lithosphere. *Geophysical Journal International*, 155: 733-748.
- 1226 Lirer, L., Pescatore, T., Booth, B. and Walker, G.P.L., 1973. Two Plinian pumice-fall deposits
1227 from Somma-Vesuvius, Italy. *Geological Society of America Bulletin*, 84: 759-772.
- 1228 Lowe, D.J., 2011. Tephrochronology and its application: A review. *Quaternary Geochronology*,
1229 6: 107-153.
- 1230 Lowe, D.J., Pearce, N.J.G., Jorgensen, M.A., Kuehn, S.C., Tryon, C.A. and Hayward, C.L.,
1231 2017. Correlating tephra and cryptotephra using glass compositional analyses and
1232 numerical and statistical methods: Review and evaluation. *Quaternary Science*
1233 *Reviews*, 175:1-44.

- 1234 Makris, J., 1978. The crust and upper mantle of the Aegean region from deep seismic
1235 soundings. *Tectonophysics*, 46: 269-284.
- 1236 Margari, V., Pyle, D.M., Bryant, C. and Gibbard, P.L., 2007. Mediterranean tephra stratigraphy
1237 revisited: Results from a long terrestrial sequence on Lesvos Island, Greece. *Journal*
1238 *of Volcanology and Geothermal Research*, 163: 34-54.
- 1239 Marinatos, S., 1939. The volcanic destruction of Minoan Crete. *Antiquity*, 13:425-439.
- 1240 Marino, G., Rohling, E.J., Rijpstra, W.I., Sangiorgi, F., Schouten, S. and Sinninghe Damsté,
1241 J.S., 2007. Aegean Sea as driver for hydrological and ecological changes in the
1242 eastern Mediterranean. *Geology*, 35: 675-678.
- 1243 Marino, G., Rohling, E.J., Sangiorgi, F., Hayes, A., Casford, J.S.L., Lotter, A.F., Kucera, M.
1244 and Brinkhuis, H., 2009. Early and middle Holocene in the Aegean Sea: interplay
1245 between high and low latitude climate variability. *Quaternary Science Reviews*, 28:
1246 3246-3262.
- 1247 McCoy, F.W., 1981. Areal distribution, redeposition and mixing of tephra within deep-sea
1248 sediments of the Eastern Mediterranean sea. In: S. Self and R.S.J. Sparks (Editors),
1249 *Tephra studies*. Nato Advanced Study Institutes Series C 75. Reidel, Dordrecht, pp.
1250 245-254.
- 1251 Mellors, R.A. and Sparks, R.S.J., 1991. Spatter-rich pyroclastic flow deposits on Santorini,
1252 Greece. *Bulletin of Volcanology*, 53: 327-342.
- 1253 Mercier, J.L., Sorel, D. and Vergely, P., 1989. Extensional tectonic regimes in the Aegean
1254 basins during the Cenozoic. *Basin Research*, 2: 49-71.
- 1255 Milner, A.M., Roucoux, K.H., Collier, R.E.L., Müller, U.C., Pross, J. and Tzedakis, P.C., 2016.
1256 Vegetation responses to abrupt climatic changes during the last interglacial complex
1257 (marine isotope stage 5) at Tenaghi Philippon, NE Greece. *Quaternary Science*
1258 *Reviews*, 154: 169-181.
- 1259 Moller, T., Schulz, H., Hamann, Y., Dellwig, O., and Kucera, M., 2012. Sedimentology and
1260 geochemistry of an exceptionally preserved last interglacial sapropel S5 in the
1261 Levantine Basin (Mediterranean Sea). *Marine Geology*, 291-294: 34-48.

- 1262 Müller, U.C., Pross, J., Tzedakis, P.C., Gamble, C., Kotthoff, U., Schmiedl, G., Wulf, S. and
1263 Christanis, K., 2011. The role of climate in the spread of modern humans into Europe.
1264 Quaternary Science Reviews, 30: 273-279.
- 1265 Narcisi, B. and Vezzoli, L., 1999. Quaternary stratigraphy of distal tephra layers in the
1266 Mediterranean - an overview. Global and Planetary Change, 21: 31-50.
- 1267 Nielsen, C.H. and Sigurdsson, H., 1981. Quantitative methods for electron microprobe
1268 analysis of sodium in natural and synthetic glasses. American Mineralogist, 66: 547-
1269 552.
- 1270 Ninkovich, D. and Heezen, B.C., 1965. Santorini tephra, Proceedings of the Seventeenth
1271 Symposium of the Colston Research Society. Colston Research Papers 17
1272 Butterworths Scientific Publications, London, pp. 413-452.
- 1273 Ninkovich, D. and Heezen, B.C., 1967. Physical and chemical properties of volcanic glass
1274 shards from Pozzuolana Ash, Thera Island, and from Upper and Lower Ash Layers in
1275 Eastern Mediterranean deep-sea sediments. Nature, 213: 582-584.
- 1276 Pichler, H. and Friedrich, W., 1976. Radiocarbon dates of Santorini volcanics. Nature, 262:
1277 373-374.
- 1278 Pross, J., Kotthoff, U., Müller, U., Peyron, O., Dormoy, I., Schmiedl, G., Kalaitzidis, S. and
1279 Smith, A.M., 2009. Massive perturbation in terrestrial ecosystems of the Eastern
1280 Mediterranean region associated with the 8.2 kyr B.P. climatic event. Geology, 37:
1281 887-890.
- 1282 Pross, J., Koutsodendris, A., Christanis, K., Fischer, T., Fletcher, W.J., Hardiman, M.,
1283 Kalaitzidis, S., Knipping, M., Kotthoff, U., Milner, A.M., Müller, U.C., Schmiedl, G.,
1284 Siavalas, G., Tzedakis, P.C. and Wulf, S., 2015. The 1.35-Ma-long terrestrial climate
1285 archive of Tenaghi Philippon, northeastern Greece: Evolution, exploration and
1286 perspectives for future research. Newsletters on Stratigraphy, 48: 253-276.
- 1287 Rach, O., Brauer, A., Wilkes, H. and Sachse, D., 2014. Delayed hydrological response to
1288 Greenland cooling at the onset of the Younger Dryas in western Europe. Nature
1289 Geoscience, 7: 109-112.

- 1290 Reck, H., 1936. Santorini: Der Werdegang eines Inselvulkans und sein Ausbruch 1925-1928.
1291 Verlag von Dietrich Reimer, Berlin.
- 1292 Regattieri, E., Giaccio, B., Nomade, S., Francke, A., Vogel, H., Drysdale, R.N., Perchiazzi, N.,
1293 Wagner, B., Gemelli, M., Mazzini, I., Boschi, C., Galli, P. and Peronace, E., 2017. A
1294 Last Interglacial record of environmental changes from the Sulmona Basin (central
1295 Italy). *Palaeogeography, Palaeoclimatology, Palaeoecology*, 472: 51-66.
- 1296 Roeser, P.A., Franz, S.O., Litt, t., Ülgen, U.B., Hilgers, A., Wulf, S., Wennrich, V., Ön, S.A.,
1297 Viehberg, F., Cagatay, N. and Melles, M., 2012. Lithostratigraphic and
1298 geochronological framework for the paleoenvironmental reconstruction of the last ~36
1299 ka cal BP from a sediment record from Lake Iznik (NW Turkey). *Quaternary*
1300 *International*, 274: 73-87.
- 1301 Rohling, E.J., Cane, T.R., Cooke, M., Sprovieri, M., Bouloubassi, I., Emeis, K.C., Schiebel, R.,
1302 Kroon, D., Jorissen, F.J., Lorre, A. and Kemp, A.E.S., 2002. African monsoon
1303 variability during the previous interglacial maximum. *Earth and Planetary Science*
1304 *Letters*, 202: 61-75.
- 1305 Rohling, E.J., Sprovieri, M., Cane, T.R., Casford, J.S.L., Cooke, M., Bouloubassi, I., Emeis,
1306 K.C., Schiebel, R., Hayes, A., Jorissen, F.J. and Kroon, D., 2004. Reconstructing past
1307 planktic foraminiferal habitats using stable isotope data: a case history for
1308 Mediterranean sapropel S5. *Marine Micropaleontology*, 50: 89-123.
- 1309 Rotolo, S.G., Scaillet, S., La Felice, S. and Vita-Scaillet, G., 2013. A revision of the structure
1310 and stratigraphy of pre-Green Tuff ignimbrites at Pantelleria (Strait of Sicily). *Journal*
1311 *of Volcanology and Geothermal Research*, 250: 61-74.
- 1312 Santacroce, R., Cioni, R., Marianelli, P., Sbrana, A., Sulpizio, R., Zanchetta, G., Donahue,
1313 D.J. and Joron, J.L., 2008. Age and whole rock-glass compositions of proximal
1314 pyroclastics from the major explosive eruptions of Somma-Vesuvius: A review as a
1315 tool for distal tephrostratigraphy. *Journal of Volcanology and Geothermal Research*,
1316 177: 1-18.

- 1317 Satow, C., Tomlinson, E.L., Grant, K.M., Albert, P.G., Smith, V.C., Manning, C.J., Ottolini, L.,
1318 Wulf, S., Rohling, E.J., Lowe, J.J., Blockley, S.P.E. and Menzies, M.A., 2015. A new
1319 contribution to the Late Quaternary tephrostratigraphy of the Mediterranean: Aegean
1320 Sea core LC21. *Quaternary Science Reviews*, 117: 96-112.
- 1321 Scaillet, S., Vita-Scaillet, G. and Rotolo, S.G., 2013. Millennial-scale phase relationships
1322 between ice-core and Mediterranean marine records: insights from high-precision
1323 $^{40}\text{Ar}/^{39}\text{Ar}$ dating of the Green Tuff of Pantelleria, Sicily Strait. *Quaternary Science*
1324 *Reviews*, 78: 141-154.
- 1325 Schmitt, A.K., Danišik, M., Evans, N.J., Siebel, W., Kiemele, E., Aydin, F. and Harvey, J.C.,
1326 2011. Acigöl rhyolitic field, Central Anatolia (part 1): high-resolution dating of eruption
1327 episodes and zircon growth rate. *Contributions to Mineralogy and Petrology*, 162:
1328 1215-1231.
- 1329 Schwarz, M., 2000. Tephrokorrelation im östlichen Mittelmeer (Meteor M40/4 Kerne). Diploma
1330 thesis, Albert-Ludwigs-Universität Freiburg, 257 pp.
- 1331 Schwarz, M., Kraml, M. and Keller, J., 1999. Tephrochronology of Meteor M40/4 cores in the
1332 Eastern Mediterranean. EUG 10 Strasbourg (France) 1999, *Terra Nova* 10 Abstract
1333 Supplement 1, *Journal of Conference Abstracts*, 4: 178-179.
- 1334 Simmons, J.M., Cas, R.A.F., Druitt, T.H. and Folkes, C.B., 2016. Complex variations during a
1335 caldera-forming Plinian eruption, including precursor deposits, thick pumice fallout, co-
1336 ignimbrite breccias and climactic lag breccias: The 184 ka Lower Pumice 1 eruption
1337 sequence, Santorini, Greece. *Journal of Volcanology and Geothermal Research*, 324:
1338 200-219.
- 1339 Smith, P.E., York, D., Chen, Y., Evensen, N.M. and Walter, R.C., 1996. ^{40}Ar - ^{39}Ar dating of
1340 Late Pleistocene volcanic glass from Santorini: a Thera Hyalo-Sphenochron. *EOS*,
1341 *Transactions, American Geophysical Union*, 77(46).
- 1342 Sparks, R.S.J. and Wilson, C.J.N., 1990. The Minoan deposits: a review of their characteristics
1343 and interpretation. In: D.A. Hardy (Editor), *Thera and the Aegean World III*. The Thera
1344 Foundation, London, pp. 89-99.

- 1345 St. Seymour, K.S., Christanis, K., Bouzinos, A., Papazisimou, S., Papatheodorou, G., Moran,
1346 E. and Dénès, G., 2004. Tephrostratigraphy and tephrochronology in the Philippi peat
1347 basin, Macedonia, Northern Hellas (Greece). *Quaternary International*, 121: 53-65.
- 1348 Sullivan, D.G., 1988. The discovery of Santorini Minoan tephra in western Turkey. *Nature*,
1349 333: 552-554.
- 1350 Sulpizio, R., Alcicek, M.C., Zanchetta, G. and Solari, L., 2013. Recognition of the Minoan
1351 tephra in the Acigöl Basin, western Turkey: implications for inter-archive correlations
1352 and fine ash dispersal. *Journal of Quaternary Science*, 28(4): 329-335.
- 1353 Tartaris, A.A., 1964. The Eocene in the semi-metamorphosed basement of Thera Island.
1354 *Bulletin of the Geological Society of Greece*, 6: 232-238.
- 1355 Thorarinsson, S., 1944. Tefrokronologiska studier pa Island. *Geografiska Analer*: 1-215.
- 1356 Tomlinson, E.L., Smith, V.C., Albert, P.G., Aydar, E., Civetta, L., Cioni, R., Cubukcu, E.,
1357 Gertisser, R., Isaia, R., Menzies, M.A., Orsi, G., Rosi, M. and Zanchetta, G., 2015. The
1358 major and trace element glass compositions of the productive Mediterranean volcanic
1359 sources: tools for correlating distal tephra layers in and around Europe. *Quaternary
1360 Science Reviews*, 118: 48-66.
- 1361 Vakhrameeva, P., Koutsodendris, A., Wulf, S., Fletcher, W.J., Appelt, O., Knipping, M.,
1362 Gertisser, R., Trieloff, M. and Pross, J., 2018. The cryptotephra record of the Marine
1363 Isotope Stage 12 to 10 interval (460-335 ka) at Tenaghi Philippon, Greece: Exploring
1364 chronological markers for the Middle Pleistocene of the Mediterranean region.
1365 *Quaternary Science Reviews*, 200: 313-333.
- 1366 Vakhrameeva, P., Wulf, S., Koutsodendris, A., Tjallingii, R., Fletcher, W.J., Appelt, O., Ludwig,
1367 T., Knipping, M., Trieloff, M., and Pross, J., 2019. Eastern Mediterranean volcanism
1368 during Marine Isotope Stages 9 to 7e (335–235 ka): Insights based on cryptotephra
1369 layers at Tenaghi Philippon, Greece. *Journal of Volcanology and Geothermal
1370 Research*, 380: 31-47.

- 1371 Vespa, M., Keller, J. and Gertisser, R., 2006. Interplinian explosive activity of Santorini volcano
1372 (Greece) during the past 150,000 years. *Journal of Volcanology and Geothermal*
1373 *Research*, 153: 262-286.
- 1374 Vinci, A., 1985. Distribution and chemical composition of tephra layers from Eastern
1375 Mediterranean abyssal sediments. *Marine Geology*, 64: 143-155.
- 1376 Vitaliano, C.J. and Vitaliano, D.B., 1974. Volcanic Tephra on Crete. *American Journal of*
1377 *Archaeology*, 78(1): 19-24.
- 1378 Wastegard, S., Gudmundsdóttir, E., Lind, E.M., Timms, R.G.O., Björck, S., Hannon, G.E.,
1379 Olsen, J. and Rundgren, M., 2018. Towards a Holocene tephrochronology for the
1380 Faroe Islands, North Atlantic. *Quaternary Science Reviews*, 195: 195-214.
- 1381 Watkins, N.D., Sparks, R.S.J., Sigurdsson, H., Huang, T.C., Federman, A., Carey, S. and
1382 Ninkovich, D., 1978. Volume and extent of the Minoan tephra from Santorini volcano:
1383 new evidence from deep-sea cores. *Nature*, 271: 122-126.
- 1384 Watts, W.A., Allen, J.R.M. and Huntley, B., 1996. Vegetation history and palaeoclimate of the
1385 last glacial period at Lago Grande di Monticchio, southern Italy. *Quaternary Science*
1386 *Reviews*, 15: 133-153.
- 1387 Wulf, S., Kraml, M., Kuhn, T., Schwarz, M., Inthorn, M., Keller, J., Kuscu, I. and Halbach, P.,
1388 2002. Marine tephra from the Cape Riva eruption (22 ka) of Santorini in the Sea of
1389 Marmara. *Marine Geology*, 183: 131-141.
- 1390 Wulf, S., Brauer, A., Kraml, M., Keller, J. and Negendank, J.F.W., 2004. Tephrochronology of
1391 the 100 ka lacustrine sediment record of Lago Grande di Monticchio (southern Italy).
1392 *Quaternary International*, 122: 7-30.
- 1393 Wulf, S., Keller, J., Paterne, M., Mingram, J., Lauterbach, S., Opitz, S., Sottili, G., Giaccio, B.,
1394 Albert, P.G., Satow, C., Tomlinson, E.L., Viccaro, M. and Brauer, A., 2012. The 100-
1395 133 ka record of Italian explosive volcanism and revised tephrochronology of Lago
1396 Grande di Monticchio. *Quaternary Science Reviews*, 58: 104-123.
- 1397 Wulf, S., Ott, F., Slowinski, M., Noryskiewicz, A.M., Dräger, N., Martin-Puertas, C., Czymzik,
1398 M., Neugebauer, I., Dulski, P., Bourne, A.J., Blaszkiewicz, M. and Brauer, A., 2013.

1399 Tracing the Laacher See Tephra in the varved sediment record of the Trzechowskie
1400 palaeolake in central Northern Poland. *Quaternary Science Reviews*, 76: 129-139.

1401 Wulf, S., Hardiman, M.J., Staff, R.A., Koutsodendris, A., Appelt, O., Blockley, S.P.E., Lowe,
1402 J.J., Manning, C.J., Ottolini, L., Schmitt, A.K., Smith, V.C., Tomlinson, E.L.,
1403 Vakhrameeva, P., Knipping, M., Kotthoff, U., Milner, A.M., Müller, U.C., Christanis, K.,
1404 Kalaitzidis, S., Tzedakis, P.C., Schmiedl, G. and Pross, J., 2018. The marine isotope
1405 stage 1-5 cryptotephra record of Tenaghi Philippon, Greece: Towards a detailed
1406 tephrostratigraphic framework for the Eastern Mediterranean region. *Quaternary
1407 Science Reviews*, 186: 236-262.

1408 Zanchetta, G., Sulpizio, R., Roberts, N., Cioni, R., Eastwood, W.J., Siani, G., Caron, B.,
1409 Paterne, M. and Santacroce, R., 2011. Tephrostratigraphy, chronology and climatic
1410 events of the Mediterranean basin during the Holocene: An overview. *The Holocene*,
1411 21(1): 33-52.

1412

1413 **Table 1:** Summary of analytical setups (voltage, beam current, and beam size) for glass
1414 compositional data of Santorini tephra used for proximal-distal marine correlations.

Laboratory	Instrument	Analytical setup	Glass standards	Samples analysed	Reference
GFZ Potsdam (WDS)	JEOL-JXA8320	15 kV, 10 nA, 5-10 µm	ATHO-G, StHs6/80, GOR-132, Lipari obs.	SAN15 (proximal)	This study
NHM London (WDS)	CAMECA-SX100	20 kV, 20 nA, 10 µm	ATHO-G, StHs6/80	SAN16, SAN17 (proximal: M9, V, M8, MV, CCT)	This study
Oxford University (WDS)	JEOL-JXA8600	15 kV, 6 nA, 10 µm	ATHO-G, StHs6/80	- LC21 (marine tephra) - MIN, CR, USC2, USC1, V (proximal)	Satow et al. (2015) Tomlinson et al. (2015)
Freiburg University (WDS)	CAMECA-SX100	15 kV, 10 nA, 10 µm	KN18	KL49, KL51 (marine tephra), unpublished proximal tephra data	Schwarz (2000)

1415

1416 **Table 2:** Summary of ages and glass geochemistries of Plinian (in bold) and Inter-Plinian Santorini eruptive events and their attribution to primary
 1417 distal marine correlatives. Well-dated tephra layers from Italy (Y-5) and Kos (W-3) are also included as chronostratigraphic information. BA =
 1418 basaltic andesitic, A = andesitic, TrA = trachyandesitic, D = dacitic, TrD = trachydacitic, RD = rhyodacitic, R = rhyolitic.

Eruption	Glass geochemistry	Core depth KL49 (cm)	Core depth LC21 (cm)	Core depth KL51 (cm)	Age (cal a BP) with 2σ uncertainty	Age reference
Minoan	R	15-59 (Z-2)	71.6-94.0 (Z-2)	-	3,563 \pm 13	Friedrich et al. (2006)
Cape Riva	R	172.5-202 (Y-2)	-	-	22,024 \pm 642	Bronk Ramsey et al. (2015)
M11b (Cape Tripiti?)	D-RD	242-249 (Y-4)	377.5 (Y-4)	-	27,480 \pm 1440	Satow et al. (2015)
Campanian Ignimbrite + M11b (2 events)?	Tr-P	344-349.5 (Y-5)	479.5-492.5 (Y-5)	90-92.5 (Y-5)	39,850 \pm 140	Giaccio et al. (2017b)
M11b?	D, RD	-	-	-	-	-
M11b?	RD-TrD	362-365.5	-	-	41,620 \pm 260	This study
M11b?	RD-(TrD)	400-401.5	-	-	46,520 \pm 590	This study
M11a?	A-D	564-566	-	-	69,590 \pm 2140	This study
M11a (2 events)?	D, A	572-578.5	-	-	70,440 \pm 2200	This study
M11a?	D	580.5-582.5	-	-	70,720 \pm 2220	This study
M11a?	A	623-627	-	-	76,470 \pm 2610	This study
Upper Scoriae 2?	A, D	660-663.5 (X-1)	-	-	?	-
Upper Scoriae 1	A	663.5-668.5 (X-1)	-	-	80,800 \pm 2900	This study
+ Megalo Vouno?	+ BA	-	-	-	-	-
USC1 precursory?	A	679 (Intra-S3)	-	-	83,540 \pm 2900	This study
USC1 precursory?	D-TrD	680 (Intra-S3)	-	-	83,800 \pm 2900	This study
M9-2	A-BA	-	957.5	346.8 (Intra-S5)	121,830 \pm 2900	This study
Vourvoulos	D-TrD	-	970.9	-	126,510 \pm 2920	Satow et al. (2015)
M8-8 (MSF)?	A-D	-	-	447-448 cm	138,720 \pm 2680	This study
Middle Pumice	A-D	-	-	452.5-455 cm (W-2)	141,040 \pm 2630	This study
M7?	A	-	-	466 cm	144,320 \pm 2560	This study
M7?	A-D	-	-	482 cm	150,490 \pm 2430	-
Cape Thera	A-D	-	1077-1119 (?)	498.5 cm	156,860 \pm 2290	This study
					152,590 \pm 9320	Satow et al. (2015)
Kos Plateau Tuff	High-silica R	-	1234.5-1246.5	507-510 (W-3)	161,300 \pm 2200	Smith et al. (1996)
Lower Pumice 2	R	-	-	553-559.5 (V-1)	176,700 \pm 590	This study
M5?	R-RD	-	-	590-591	185,080 \pm 710	This study
Lower Pumice 1	R-RD	-	-	592-594 (V-3)	185,740 \pm 720	This study
Cape Therma 3	TrA/A-TrD/D	-	-	637-639.5 (Intra-S7)	200,210 \pm 880	This study

1419

1420 **Table 3:** Revised Eastern Mediterranean marine tephrostratigraphy for the past 200 kyrs.

Tephra	Volcanic centre	Eruptive event	Dispersal	Age (ka)	Dating method	Age reference
Z-1	Somma-Vesuvius	Pompeii	SSE	AD79	Historical record	Lirer et al. (1973)
Z-2	Santorini	Minoan	E	3.6	¹⁴ C	Friedrich et al. (2006)
Z-3 to Z-5	Central Anatolia?	unknown	S	8-10	interpolated	McCoy (1981)
Y-1	Mount Etna	Biancavilla Ignimbrite	E	17.3 ± 0.4	¹⁴ C	Albert et al. (2013)
Y-2	Santorini	Cape Riva	N	22.0 ± 0.6	¹⁴ C	Bronk Ramsey et al. (2015)
Y-4	Santorini	Cape Tripiti/M11	SE	27.5 ± 1.4	interpolated (LC21)	Satow et al. (2015)
Y-3	Campi Flegrei	unknown	ESE	29.0 ± 0.4	¹⁴ C	Albert et al. (2015)
Y-5	Campi Flegrei	Campanian Ignimbrite	E	39.9 ± 0.1	⁴⁰ Ar/ ³⁹ Ar	Giaccio et al. (2017b)
Y-6	Pantelleria	Green Tuffs	E	45.7 ± 1.0	⁴⁰ Ar/ ³⁹ Ar	Scaillet et al. (2013)
Y-7	Ischia	Tufo Verde di Epomeo	SE	55.0 ± 2.0	⁴⁰ Ar/ ³⁹ Ar	Watts et al. (1996)
Y-8	Salina	Grey Porri Tuffs	SE	66.7 ± 2.0	interpolated	Kraml (1997)
Y-9 (former X-1)	Stromboli	Petrazza Tuffs	ENE	75.3 ± 2.0	interpolated	Kraml (1997)
X-1	Santorini	Upper Scoriae 1	S	80.8 ± 2.9	interpolated (KL49)	This study
X-4	Mount Etna	Acireale	E	89.5 ± 2.0	interpolated	Kraml (1997)
X-5	Campanian Province	Unknown	SE	106.2 ± 1.6	⁴⁰ Ar/ ³⁹ Ar	Giaccio et al. (2012)
X-6	Campanian Province	Unknown	E	109.5 ± 0.9	⁴⁰ Ar/ ³⁹ Ar	Regattieri et al. (2017)
W-0 (P-11)	Pantelleria	Ignimbrite P	E	133.5 ± 2.0	interpolated (LC21)	Satow et al. (2015)
W-1	Vico	Ignimbrite D	E	138.0 ± 2.0	K/Ar	Laurenzi and Villa (1987)
W-2	Santorini	Middle Pumice	S	141.0 ± 2.6	interpolated (KL51)	This study
W-3	Kos	Kos Plateau Tuff	S	161.3 ± 2.2	⁴⁰ Ar/ ³⁹ Ar	Smith et al. (1996)
V-0	Pantelleria	Ignimbrite S	E	171.0 ± 1.7	⁴⁰ Ar/ ³⁹ Ar	Rotolo et al. (2013)
V-1	Santorini	Lower Pumice 2	SE/SW	176.7 ± 0.6	interpolated (KL51)	This study
V-2	Roman Province	Unknown	SE	176.9 ± 2.0	interpolated	Kraml (1997)
V-3	Santorini	Lower Pumice 1	SE/SW	185.7 ± 0.7	interpolated (KL51)	This study
Intra-S7	Santorini	Cape Therma 3	SE?	200.2 ± 0.9	interpolated (KL51)	This study

1421